X-RAY FLUORESCENCE SPECTROMETRY USING SYNCHROTRON RADIATION WITH APPLICATIONS IN UNMANNED AIRCRAFT ENVIRONMENTAL SENSING

By

Sean Richard Gopal Barberie

RECOMMENDED:

Dr. Christopher R. Iceman

Dr. Michael C. Hatfield

Dr. Catherine F. Cahill
Advisory Committee Chair

Dr. Thomas Green
Chair, Department of Chemistry and Biochemistry

APPROVED:

Dr. Paul Layer
Dean, College of Natural Science and Mathematics

Dr. John Eichelberger
Dean of the Graduate School

8 December 2015
Date

X-RAY FLUORESCENCE SPECTROMETRY USING SYNCHROTRON RADIATION WITH APPLICATIONS IN UNMANNED AIRCRAFT ENVIRONMENTAL SENSING

A

THESIS

Presented to the Faculty

of the University of Alaska Fairbanks

in Partial Fulfillment of the Requirements

for the Degree of

MASTER OF SCIENCE

By

Sean Richard Gopal Barberie, B.S.

Fairbanks, Alaska

December 2015

Abstract

In this thesis I present an analytical optimization of the Synchrotron Radiation X-Ray Fluorescence (SR-XRF) technique for applications in unmanned aircraft aerosol studies. In environmental and atmospheric science, there is a pressing need for aerosol measurements at various altitudes in the atmosphere and spanning large regions. This need is currently either ignored, or met to a limited degree by studies that employ manned aircraft. There is, however, a great deal of opportunity to improve and expand on these studies using the emerging technology of unmanned aircraft systems. A newly developed aerosol sampler makes this opportunity a near-reality by its ability to collect aerosol samples in-situ from unmanned aircraft platforms. The challenge lies in analyzing these samples for elemental composition. In airborne aerosol studies, the ability to resolve where a sample was collected both spatially and temporally is limited by the sensitivity of the analysis technique. In aircraft-based aerosol collection, the length of the aerosol sample spot corresponds to distance. Thus the spatial resolution of an airborne study is limited by the amount of mass that must be collected for analysis. The SR-XRF optimizations outlined in this thesis decrease the amount of sample mass required for detectable elemental concentrations, allowing aerosol samples to be analyzed in smaller areas corresponding to smaller time steps. Since, in a flight path, time steps are directly correlated with distance, analysis of smaller time steps results in the ability to measure aerosols at higher spatial resolution. Four SR-XRF analysis configurations were experimentally tested: monochromatic beam, white beam, filtered white beam, and filtered white beam-filtered detector to determine which configuration gave the highest elemental sensitivity and selectivity. Of these tested methods, the straight polychromatic white beam configuration resulted in the best sensitivity for elements across a large range of x-ray energies for small amounts of mass collected on thin film substrates. The research in this thesis provides researchers with an optimized method for non-destructively analyzing a wide variety of environmental samples with high elemental sensitivity and selectivity. This research also has important implications for the ability to perform in-situ aerosol studies with unmanned aircraft on a systematic basis.

Table of Contents

Page

List of Figures

Page

List of Tables

Page

Acknowledgements

"Men wanted for hazardous journey, small wages, bitter cold, long months of complete darkness, constant danger, safe return doubtful, honor and recognition in case of success"

— Sir Ernest Shakelton, 1913

That quote appeared as an advertisement in a British newspaper in 1913. It was conscripted by Sir Ernest Shakelton, looking for a crew to join him on an expedition to the South Pole. In my admittedly-much-less-significant personal quest to move from California to Alaska for graduate school, I found Shakelton's description to be an apt portrayal of both my initial hesitation and my excitement at the prospect of pursuing graduate school in such an exotic and adventure-rich place. Having never lived in a place with snow on the ground, I was now moving to the top of the world, I was moving to the last frontier. Despite some initial trepidation, Alaska has been an amazing experience and opportunity for personal growth. I've lived in a cabin without running water, eaten bear meat, visited remote native villages, hiked on glaciers, skied on rivers under the northern lights, and even spent a summer living in a van. I also been able to do cutting edge research with top academic researchers at the foremost arctic research university in the world. It has been an amazing, sometimes disorienting, whirlwind of experiences.

I cannot express enough gratitude to the people who have guided me during this time, both in how to be an academic researcher, and how to live in this beautiful and unique state.

First and foremost, I want to thank Cathy Cahill, who has been my guide and mentor from the start and who was the person who first asked me to leave the familiarity of California behind and join her research team in the subarctic. She has been a constant source of reassurance and inspiration. I met Cathy at the Stanford Synchrotron Radiation Lightsource (SSRL) and SLAC National Accelerator Laboratory. I was working with her father, Tom Cahill, on setting up an experimental station to analyze particulate aerosol samples using the high energy x-ray beam from the synchrotron light source. I was at the end of my undergraduate program in physics but I very much wanted to follow through with this area of research and see where it would lead. Cathy gave me that opportunity by asking me to do a graduate program with her at University of Alaska Fairbanks: allowing me to continue doing synchrotron work with her and Chris Iceman, publish on our

accomplishments, and allowing me to explore applications in the emerging world of unmanned aircraft systems–leading to me discovering new research interests in routine data collection and managing big data problems in science. The breadth of opportunities and research areas I was able to pursue while working with Cathy (going from experimental physics clear over to applications based research in unmanned aircraft) was exactly what I wanted and needed out of a graduate program and it is something that I could probably only have had with the thoughtful and well-rounded mentorship that she provided. She guided me when I needed guidance but gave me sufficient room to explore and make my own mistakes–for that I am very grateful.

Above I mentioned Chris Iceman, I owe him gratitude as well. He was a colleague for synchrotron work and, more importantly, a friend who had arrived in Alaska a couple years before me. He had enough experience to offer advice but was still new enough to sympathize with the confusion and frustrations I sometimes felt. I also had some very fun/nerdy conversations with him about programming using the Python programming language.

I would also like to thank Mike Hatfield, Marty Rogers, Ro Bailey, Barbara Johnson, Greg Foscue and the rest of the ACUASI team. Establishing a link with the world of unmanned aircraft has definitely had a positive impact on the direction of my career and has flooded my mind with possibilities for data collection and the role of robotics in science. Mike Hatfield has gone above and beyond in agreeing to join my committee as co-chair and serve as a constant supporter and advisor. Marty Rogers, although not officially, has also taken on a role of mentorship for which I am very grateful. There were moments when what I needed most was some brutal honesty and a kick in the ass; I am comforted to know that when I'm in that position, Marty will provide the kick. Ro Bailey, Barbara Johnson, and Greg Foscue each individually took the time to learn about my background and my long-term research interests and help me find projects at ACUASI to match. I'm am grateful to them for this guidance and accommodation. It has been and continues to be a very rewarding experience to know that the work I'm doing both interests me and is useful to ACUASI as a whole. It has long been known that the people you surround yourself with fundamentally affect how you see the world and how you approach your career and your life, I could not have asked for a better group of ambitious, dedicated, competent people with whom to surround myself.

Lastly, I would like to thank my close friends, co-grad students, and neighbors who

provided comfort, social interaction, comradery, and the opportunity to leave grad school behind for a few hours and be a human: Erin Gleason, Peter Peterson, Erin Tilly, Miker Frantes, Elliot Wilson, Alexis Will, Aaron Cook, Emma Boone, Christopher Benke, Derek Starkenburg, Katia Kontar, Amy Hendricks, Catey Burtness-Adams, Juliette Funck, John Denton, Sam Vanderwaal, Amanda Barker, Corey DiRutigliano, Cassidy Saunders, and Angela Younie.

Chapter 1
Motivation & Background

1.1 Motivation

Atmospheric aerosols can adversely affect human health [1], impact global climate [2], reduce visibility [3] [4] [5], harm aircraft [6] [7] [8] [9], and deposit pollutants into sensitive ecosystems [10]. To quantify these aerosol effects there is a crucial need to know the variation of aerosol composition and concentration in space and time. Previously the only way to sample in-situ atmospheric aerosol compositions and concentrations is either with ground-based aerosol samplers, which greatly limit the available information on the vertical distribution of aerosols, or with manned aircraft, which are so costly as to make broad surveys on a systematic basis impractical. Additionally, some needed measurements are too dangerous for manned aircraft, such as attempting to get compositional data for aerosols in volcanic plumes or over forest fires. The developing technology of Unmanned Aircraft Systems (UAS, Unmanned Aerial Vehicle, UAV, or drone) provides us with a potential platform for making measurements of aerosols as they transport and transform in the atmosphere. However, few instruments have been designed to measure in-situ aerosol properties from an unmanned aircraft and those technologies that have been developed for that purpose have some limitations in the type of data that they can collect. This is in part due to the fact that the ability to develop new instruments for in-situ sampling has been constrained by the low sensitivity of available elemental analysis techniques for extracting data from the collected samples.

1.2 Aerosol Sampling

A frequently used method for collecting atmospheric aerosols is sampling with filters. Filter based sampling collects particles by pulling an air stream through a semipermeable material. As the air stream moves through the material, particles above a certain size are unable to make the passage and become lodged in the filter. Filters seem like they would be an obvious choice for unmanned aircraft sampling because they are small and lightweight, however, they present some serious limitations. A single filter will accumulate mass in the same location on the filter for the entire time that air is being drawn through it. Aboard an unmanned aircraft this would mean that a single filter sample would have an amalgamation of mass from the entire flight, i.e. it would not provide temporally-resolved data of mass and composition changes in a plume or vertical profile.

The other most common aerosol data acquisition method is the use of optical particle counters. Optical particle counters are used to both count and size the incoming particles using light scattering or light obscuration. Some light source (a laser, a halogen light, etc) is used, and as the incoming particles are passed through it, the beam of light is changed as a function of the particle size. Based on that mechanism, a quantification of both size and number can be taken. Optical particle counters are indispensable in aerosol science and have already seen use aboard unmanned aircraft [11] [12]. However, these counters do not store the sample for later analysis and they provide no primary means of determining what the observed particles are actually composed of, only their size and number. In the context of these two existing methods (filter-based sampling and optical particle counters), it becomes apparent that we need a third option that captures features from both methods. What is needed is a way to collect data on the size of the particles collected as well as the composition and concentration of those particles. This data must be collected in a way that preserves sample discrimination with respect to both the location of the aircraft at the time of sampling and over short time intervals, since the movement of the aircraft makes the data set highly non-stationary.

It was this need that motivated the development of a new aerosol sampler, the Airborne DRUM Sampler (ADS). The ADS is designed for collecting and analyzing in-situ atmospheric aerosol concentrations and compositions in the style of a cascade impactor. The development of this new sampler has evolved as a careful balance between maintaining the underlying physical principles of impaction from an experimental standpoint as well as attempting to implement the best engineering practices to create a reliable product that meets the tight constraints of UAV payload integration.

1.2.1 Aerosol Sampling with Impaction

Impactor technology itself is well-established[13] [14] [15] [16] [17]. The first modern impactor was designed in 1945 [15]; since that time the technology has seen a number of variants [18] [19]. In this section we will review the fundamentals of impaction theory and take a close look at the rotating Ludgren-style impactors, particularly the DRUM sampler, on which the ADS is based.

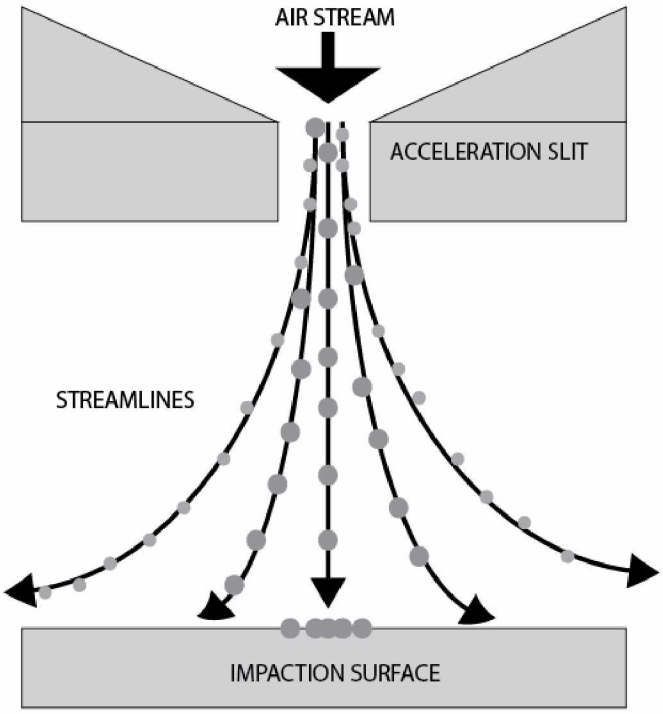

Figure 1.1. A diagram of impaction when the airstream is being passed through an accelerating passage (or slit). The heaviest particles (the middle streamlines) are unable to make the bend due to their momentum and are forced to hit the impaction surface, sticking where they land. The smaller particles (the outer streamlines) follow the airstream around the impaction plate and continue downstream.

1.2.2 Impactor Theory

Impaction is the process whereby a stream of air, confronted by a perpendicular surface, is forced to make a sharp turn. Particles large enough to have inertial forces greater than the viscous force of the fluid stick to an impaction surface or impaction plate (Fig. 1.1). Exactly which particles get forced from the stream is a function of the particle size. The particles within the air stream (shown in the figure as streamlines) above a certain size cut off have so much momentum that they are unable to follow the rest of the air stream to make the required turn. Instead, these particles continue on their inertial path and strike the impaction plate. These particles that strike and stick to the impaction plate can later be analyzed for particle mass concentrations and composition.

Since momentum is velocity times mass, varying the velocity of the air stream will change the size range of particles that will be impacted. In many impactor designs, the velocity is altered by passing the air stream through an acceleration slit before the path

diverges. The particle size in which half of the particles impact and half of the particles are carried off by the fluid is known as the cut point for that particular setup. The impactor particle size-cut points can be calculated according to the Stokes equation, which describes slit orifice impactors.

$$Stk50 = \frac{2\tau U}{D_j} = \frac{\rho_P d_P^2 U C_c}{9\eta D_j} \tag{1.1}$$

Such that $Stk50$ is the Stokes number for the rectangular jet, τ is the relaxation time, U is the nozzle exit velocity, D_j is the slot half-width (slot Length $\times$ Width^2), ρ_P is the particle density, d_P is the particle diameter, C_C is the Cunningham slip correction, and η is the viscosity of air.

The cut point dependence on air stream velocity, and therefore on the width of the acceleration slit, allows the designer of an impactor to select their cut point based on theoretical calculation using the Stokes equation. Note that, empirically, a slotted orifice will often have a Stk50 of 0.79 at atmospheric conditions and at low Reynolds numbers. The DRUM (to be discussed in the next section) is about 0.82 because the surface of impaction is curved. At high Reynolds numbers, a slot will have a Stk50 of about 0.65. The point here is that the Stk50 can be useful for theoretical considerations during impactor design, but only under certain conditions, and should always be verified empirically.

1.2.3 The DRUM Sampler

The ADS is a thorough re-design of the classical Davis Rotating-drum Universal-size-cut Monitoring (DRUM) impactor. The original DRUM sampler has some historical precedent in aerosol collection; it was designed at University of California Davis in the late 1980's by Cahill et al. [20] [21] [22]. The DRUM sampler is traditionally comprised of either three or eight stages, where each stage corresponds to a different particle size cut point. A recent redesign of the three stage version of the DRUM sampler has been performed by Bukowiecki et al. [23], often referred to in the literature as the Rotating DRUM Impactor or RDI. However, the design of the RDI diverges from that of both the DRUM and the ADS, therefore from here on we will primarily be referring to the ADS and the Cahill DRUM on which it is based.

The DRUM sampler, and the ADS by extension, are what are known as Lundgren-style impactors, in that they operates under many of the same principles as the early Lundgren

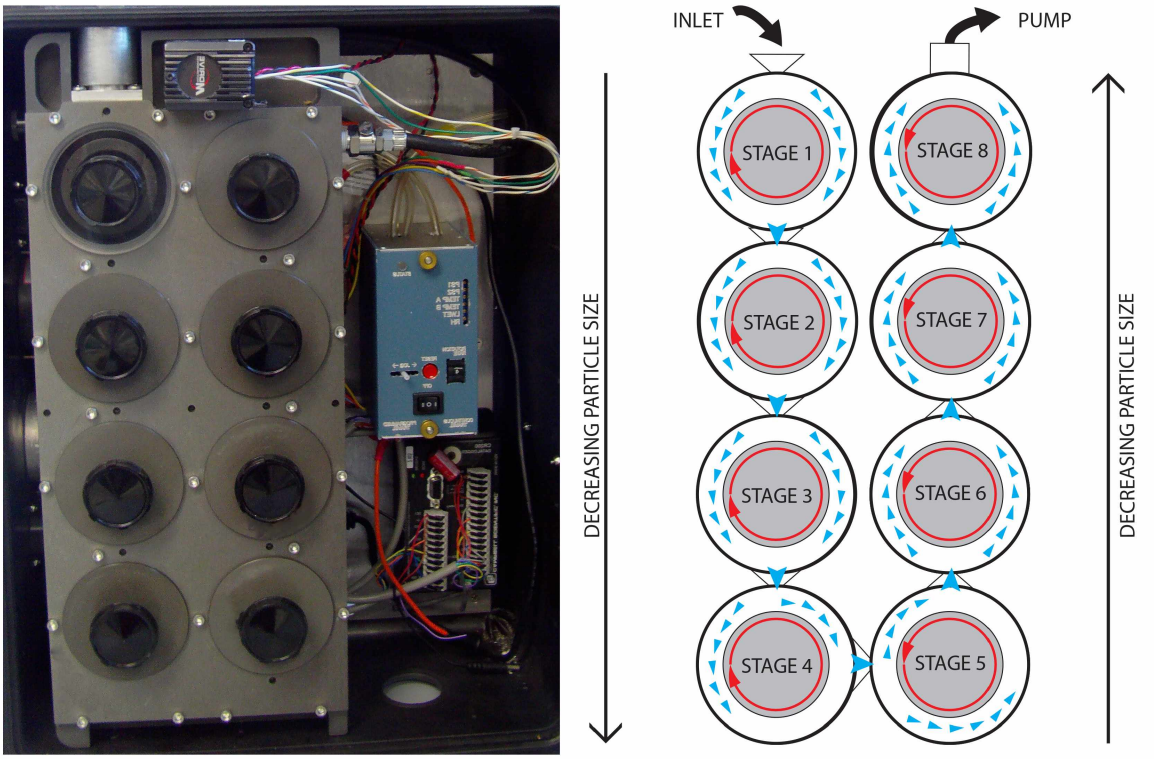

Figure 1.2. A top-down-view photo (left) and diagram (right) of the DRUM sampler. This illustration demonstrates the method of cascade impaction that is utilized in the ADS.

cascade-style impactor [24]. The principle innovation of the DRUM sampler over other impaction-based samplers is the series of rotating wheels that hold the target substrate, a Mylar film of 190 mm by 15 mm and an approximate thickness of 1.8 micrometers (Du Pont Inc.). The substrate is coated with an APIEZON-L grease to minimize particle bounce-off. An illustration of the DRUM impactor (Fig. 1.2) shows the aforementioned rotating wheels. Each stage of the impactor is subjected to a different air intake velocity due to the decrease in passage size (or slit size). Since the ADS is essentially a stacked version of the DRUM, Fig. 1.2 is useful as an illustration of the operating methods behind the ADS, since the stage-by-stage flow procedure is essentially the same between the DRUM and the ADS; while the DRUM is far easier to visualize in two dimensions.

When in operation, air enters the sampler through an optional inlet head that procures a PM10 (particulate matter of 10 micrometer in aerodynamic diameter) cut-point. As the jet stream moves into the chamber it meets a slowly rotating wheel carrying the substrate. The particles that have too much momentum to make the bend and therefore cannot follow the air stream hit the substrate and get stuck at that point. As the air is pulled through

the passage between the first and second stage, it must pass through a small slit-shaped opening that acts to increase the velocity of the stream on the other side. Thus stage 2 can capture particles smaller than those that are vulnerable to stage 1 because the particles experience an increased momentum. The effect is that the cut-point of stage 2 is now lower (that is, it can capture smaller particles) than that of stage 1. This trend continues as the air stream progresses through each chamber, where each stage impacts smaller and smaller particles. The output at the end of the chain of stages is where the vacuum is connected so that it can draw air through the sampler.

1.2.4 Analysis

High sensitivity analyses are crucial for the samples that will result from this sampler. The samples themselves can be of such low mass that discrimination by elemental concentration using some methods (e.g. x-ray fluorescence using an x-ray tube, electron probe microanalysis) will be impossible. Additionally, since each small turn of the impaction wheel corresponds to a new sample taken at a new location, this sampler will produce a very large number of spots that require analyses, making other methods impractical (e.g. neutron activation analysis, mass spectrometry). The most viable option is that the analysis be performed using a refined version of the existing synchrotron radiation based analytical method that has been used in the past for DRUM and RDI samples, with numerous examples in the literature [25] [26] [27] [28] [29] [30] [31] [32] [33] [34].

1.2.5 Synchrotron Lightsources

Synchrotron radiation x-ray fluorescence (SR-XRF) requires the use of a synchrotron lightsource. Synchrotron lightsources are large ring-shaped accelerators that generate electromagnetic radiation in the x-ray regime. This emitted radiation is known as synchrotron radiation and ranges from the far infrared to hard x-rays and even gamma rays. Synchrotrons generate this radiation by accelerating charged particles (electrons or positrons) to highly relativistic speeds inside a containment ring. The charged particles are forced to move in the circular path of the ring by large bending magnets, creating a constant acceleration of the charged particles towards the center as with any centripetal acceleration. From electromagnetism, it is well known that any charged particle undergoing acceleration must give off energy; accordingly, the charged particles in the synchrotron storage ring give off

synchrotron radiation in the form of x-ray photons. These x-rays escape the ring tangentially down the beamlines to be used for experiments at the end-station instrumentation of the researchers. Additionally, wigglers or undulators can be placed in straight sections of the ring to cause the charged particles to shake or vibrate, giving off additional x-rays. Synchrotron lightsources are advantageous over traditional x-ray tubes because they generate photon fluxes that are many orders of magnitude greater those generated by x-ray tubes. A diagram of a synchrotron is shown in Figure 1.3.

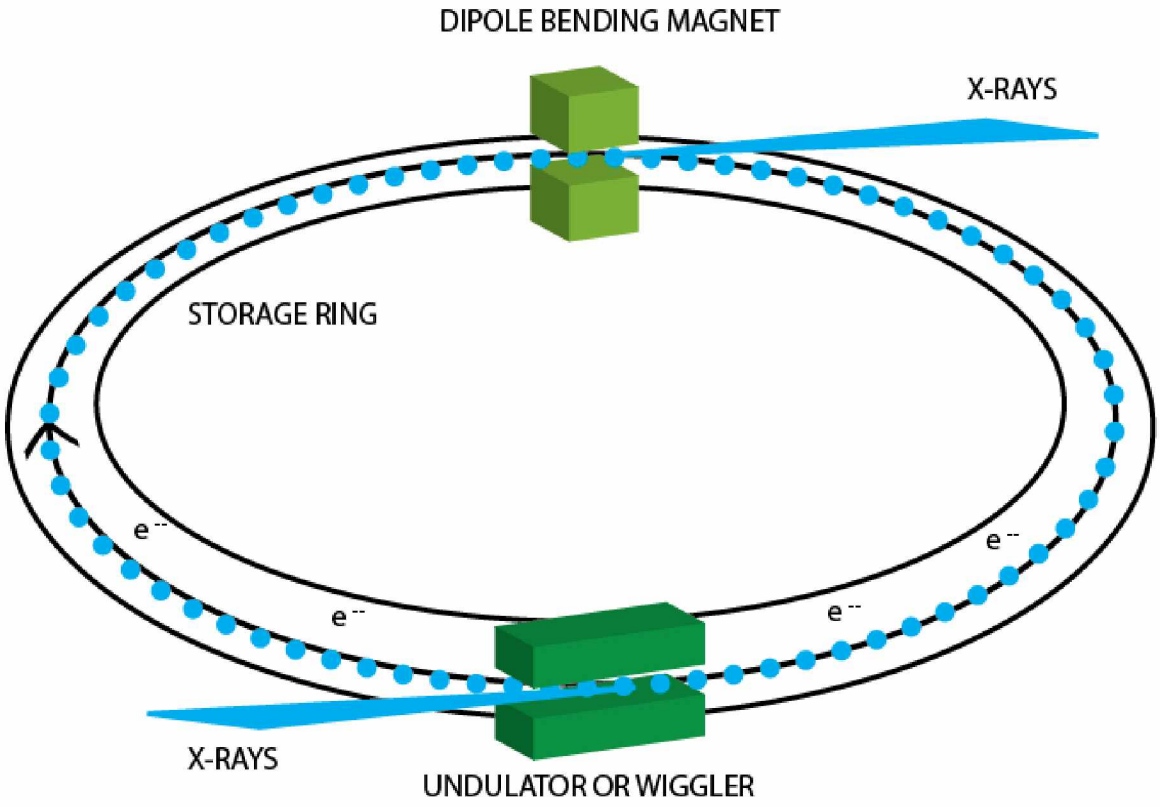

Figure 1.3. Shown here is a illustration of a synchrotron lightsource and the fundamental process by which it generates synchrotron radiation. Electrons are accelerated in the storage ring and passed through bending magnets and undulators. X-rays are emitted and passed down beamlines for use in experiments.

1.2.6 X-Ray Fluorescence

X-ray fluorescence is the process by which SR-XRF works. The electrons in the orbital shells of atoms exist in discrete energy levels. If an electron is ejected from one of the inner orbital shells, it will cause an outer-shell electron to drop down and fill the vacated hole.

When this occurs, an electron from an even further out shell will drop down to fill the space vacated by that electron and so on, with the process continuing in a cascade until the inner shells are filled. When an electron drops down into an inner shell, it will give off a photon of the energy difference between the two levels, usually about 103 to 105 electron volts (eV). This energy range corresponds to photon wavelengths of 10 nm to 10^{-2} nm, which means that the emitted photons are x-rays. The difference in energy for the various levels and thus the energies of the emitted x-rays, are unique and can be used to identify the element in which that transition occurred. Since these x-rays are characteristic of the type of atom from which they were emitted, they are known as *characteristic* x-rays.

In SR-XRF, we use the high energy photons from a synchrotron light source like the Stanford Synchrotron Radiation Lightsource (SSRL) at SLAC to ionize electrons from the inner shells causing this cascade process to occur. We are then able to detect the characteristic x-rays that result and by their energies identify the elements of origin. As this is performed on a sample, the many transitions that occur produce a wealth of characteristic x-rays that are collected by a detector to produce a characteristic x-ray spectrum. From this spectrum we can determine the quantities of given elements within the sample by comparing results to a standard-generated yield curve. This is how SR-XRF is able to determine the composition of unknown materials.

1.3 Unmanned Aircraft Systems

A particularly important emerging technology for these types of environmental studies are unmanned aircraft systems (UAS, also known as unmanned aerial vehicles, UAVs, or drone). Although unmanned aircraft have existed for some time, they are now finally making the transition from a purely military technology to an area of active application-based research in the commercial and academic sectors. This technology is poised to become an exceedingly valuable tool to researchers for scientific data collection, particularly with regard to environmental sensing (both remote and in-situ).

[1]Terminology: *unmanned aircraft system* (UAS) generally refers to aircraft without an onboard pilot but including a ground control station, necessary communication networks, and an operator (albeit on the ground and not in the aircraft). *Unmanned aerial vehicle* (UAV) refers to the unmanned aircraft that is a component of the unmanned aircraft system. Colloquially and especially in the media, unmanned aircraft are referred to simply as *drones*.

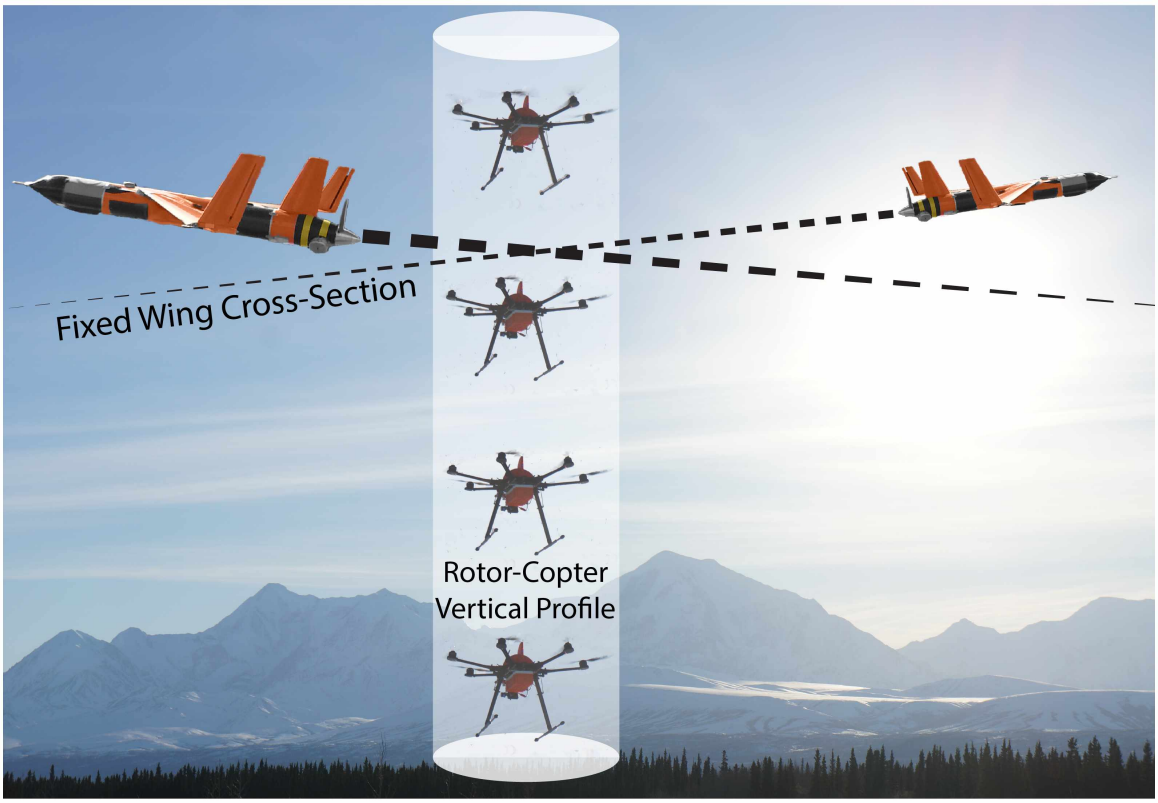

Figure 1.4. This illustration shows two approaches to environmental sensing with the two configurations of unmanned aircraft: cross-sectional studies using fixed-wing UAS, and vertical profiles using rotor-based UAS.

1.3.1 UAS Characteristics & Classifications

UAS are examples of autonomous, semi-autonomous, or remotely piloted aircraft. They have either a pre-programmed flight plan, receive real-time commands from an operator over a com-link, or are controlled by some combination of the two. To be considered a UAS the craft must be powered, as gliders are not considered unmanned aircraft for regulatory purposes.

There are two main UAS configurations: fixed wing (airplane-like) and rotor-driven (multi-rotors, helicopters, quad-copters, etc), examples of each are shown in Figure 1.4. UAVs can range in size from small insect sized nano drones to aircraft as big as large private jets, such as the MQ-9 Predator2/Reaper with a 65 ft wingspan and a maximum take-off weight of 10,000 pounds. As for establishing official categories for further classification, there is a lot of debate as to where the lines should be drawn and exactly what variables

should determine a category (e.g. size, weight, flight endurance, intended purpose, mission types). Even within the U.S. military the categorization of unmanned aircraft differs between the Air Force, Army, and Marine Corps. It is likely that as UAV use in the civil sector increases, the market will establish its own categorization simply by what is most useful. Some of the more established size classes, though, are: micro (<0.9 kg), mini (0.9-13.6 kg), tactical (13.6-454.5 kg), medium altitude - long endurance (abbreviated *MALE*, 454.5-13,636.4 kg), and high altitude - long endurance (abbreviated *HALE*, >13,636.4 kg).

One of the most discussed (and firmly established) size classes right now is the sUAS or small UAS class. This category includes all unmanned aircraft under 25 kilograms (55 lbs). Most civilian UAVs are likely to fall in this range. These platforms are likely to have the largest impact in non-military sectors (civil, industry, academic, research), due to their relatively low cost and their potential for simpler regulatory constraints resulting from the FAA Modernization and Reform Act of 2012 (discussed in the next subsection).

1.3.2 Regulatory Considerations & The FAA Test Sites

On February 14th of 2012, President Barack Obama signed bill HR658, the FAA Modernization and Reform Act of 2012 (FAAMRA). This bill outlines benchmarks and provisions for integrating civil UAS into the national airspace system (NAS) by September 30th, 2015. This move was in response to the increasingly apparent reality that current FAA regulations were insufficient to deal with the rapid expansion of interest in using UAS in the NAS. That insufficiency of proper regulation has been an impediment for fully utilizing UAS in environmental sensing [35]. Some experts have concluded that the lack of regulatory framework is also holding back the development of the UAV civilian sector and that it will continue to do so until a stable framework for routine UAS operation is established [36]. Along the same lines, the FAA anticipates that within five years of establishing a regulatory framework, approximately 10,000 civilian UAS ventures will begin operations [37].

FAAMRA begins the process of establishing a formal and fully-functional regulatory framework for allowing UAS to fly for civil purposes in the NAS. It requires the FAA to issue regulations pertaining to the operation of sUAS and requires the FAA to form and implement a plan to begin integration of UAVs into the NAS. As a step towards that goal, the FAAMRA establishes six test sites throughout the United States specifically for the study of technical and logistical issues that may arise from the integration of UAS into the NAS (Fig.

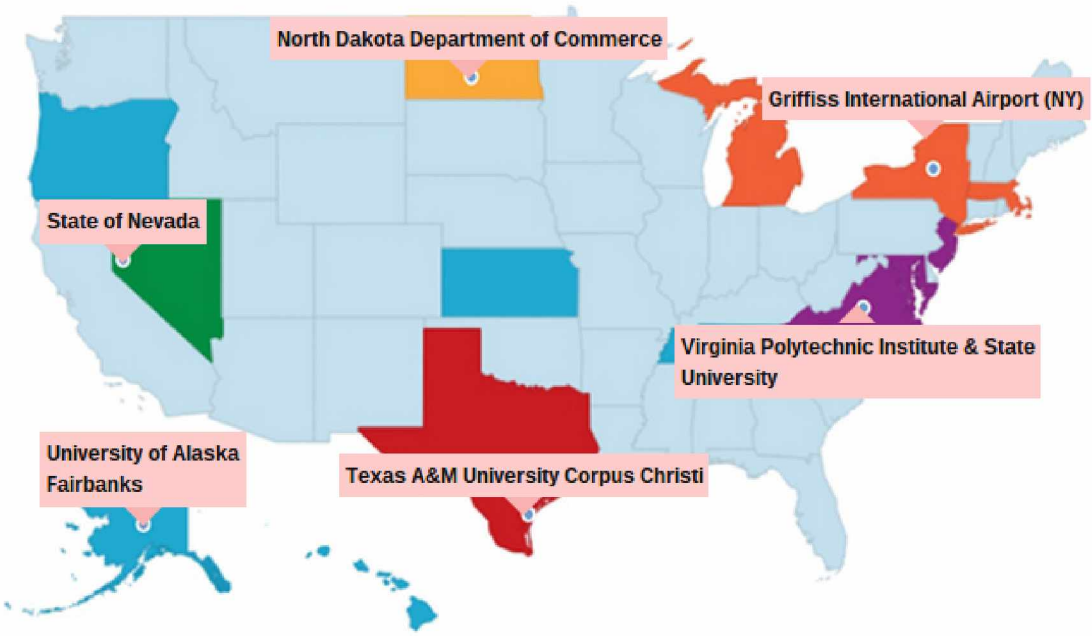

Figure 1.5. This figure displays the six FAA unmanned aircraft test sites. These test sites were established throughout the United States by the FAA Modernization and Reform Act of 2012 for study technical and logistical issues that may arise from the integration of unmanned aircraft into the national airspace. Figure courtesy of the FAA website.

1.5). The most prominent of these six test sites is the Pan-Pacific UAS Test Range Complex (PPUTRC) with test ranges in Alaska, Hawaii, and Oregon. The PPUTRC is a subsidiary of the Alaska Center for UAS Integration and the University of Alaska Fairbanks. This test site is particularly valuable to assessing the complication of integrating UAS into the NAS because it spans seven different climactic zones and tests the use of unmanned aircraft in remote locations with limited infrastructure, a realm where UAS may have a great deal of societal value. The other fives FAA test sites are managed by: The State of Nevada, New York's Griffiss International Airport with ranges in Massachusetts and Michigan, North Dakota Department of Commerce, Texas AM University Corpus Christi, Virginia Polytechnic Institute and State University with ranges in New Jersey and Maryland.

In addition to establishing the test sites, the FAAMRA mandated some other items of note:

- A mandate for the development and designation of permanent areas in the Arctic where small UAV may fly for commercial and research purposes. This area would

include beyond line-of-sight flights.

- A mandate for an exemption from rules and regulations for model/hobby aircraft weighing less than 55 lbs when flown within line-of-sight.
- A mandate requiring the development and implementation of operating and certification requirements for UAS by the end of 2015.
- A mandate for the establishment of a simplified process of issuing authorizations for UAS flights in the NAS.
- A commitment to incrementally increasing airspace access as use-experience and safety data area accumulated, as well as to facilitate public agency use of the UAS test sites.

The participation of the University of Alaska Fairbanks (UAF) in the test site program has opened the door to UAF conducting more research flights and developing and testing new payloads.

Advances in UAS technology have shown great promise in the realm of scientific data collection. Most of these advances have taken place with regards to the platforms themselves: reduced cost of a UAS, improved flight safety [38], standardized and simplified flight controls, and improvements in autopilots [39] [40]. At the same time, UAS have seen a number of improvements in integration and miniaturization of sensors such as hyper-spectral cameras, synthetic aperture radar, lidar, thermal cameras, and atmospheric sensors. Even without these advanced sensing systems, UAS present some useful off-the-shelf capabilities. The integrated GPS receiver can measure the absolute aircraft position and airspeed. The micro-inertial navigation system can measure the aircraft altitude. The on-board microprocessor and flight data recorder handle flight control and data logging. Most UAS are even equipped with a camera system (often a GoPro in newer model sUAS). The introduction of UAS technology into science, particularly with sampling innovations like the ADS, may open up new possibilities for the breadth and frequency of environmental data collection and drastically changes the landscape of the types of scientific studies that are possible and manageable.

1.4 This Thesis

My thesis focuses on experiments in x-ray fluorescence spectrometry using synchrotron radiation with applications in unmanned aircraft environmental sensing. I will discuss the development of a means of collecting material aerosol samples and analyzing them with sufficient sensitivity to allow for unmanned aircraft to do the work. Although the development of the analytical technique itself is complete (discussed in chapters 2 and 3), the development of the prototype aerosol sampler ran into time consuming impediments so it will be some time still before it can be tested on an unmanned aircraft.

1.5 References

[1] PN Breysse, RJ Delfino, F Dominici, ACP Elder, MW Frampton, JR Froines, AS Geyh, JJ Godleski, DR Gold, and PK Hopke. Us epa particulate matter research centers: summary of research results for 2005âĂŞ2011. *Air Quality, Atmosphere and Health*, 6(2):333–355, 2013.

[2] TF Stocker, D Qin, G Plattner, M Tignor, SK Allen, J Boschung, A Nauels, Y Xia, V Bex, and PM Midgley. Climate change 2013. the physical science basis. working group i contribution to the fifth assessment report of the intergovernmental panel on climate change-abstract for decision-makers. 2013.

[3] JL Hand, BA Schichtel, M Pitchford, WC Malm, and NH Frank. Seasonal composition of remote and urban fine particulate matter in the united states. *Journal of Geophysical Research: Atmospheres*, 117(D5), 2012.

[4] WC Malm, JV Molenar, RA Eldred, and JF Sisler. Examining the relationship among atmospheric aerosols and light scattering and extinction in the grand canyon area. *Journal of Geophysical Research: Atmospheres (1984âĂŞ2012)*, 101(D14):19251–19265, 1996.

[5] WC Malm, JF Sisler, D Huffman, RA Eldred, and TA Cahill. Spatial and seasonal trends in particle concentration and optical extinction in the united states. *Journal of Geophysical Research: Atmospheres*, 99(D1):1347–1370, 1994.

[6] TJ Casadevall. The 1989-1990 eruption of redoubt volcano, alaska: impacts on aircraft operations. *Journal of Volcanology and Geothermal Research*, 62(1):301–316, 1994.

[7] M Guffanti, JW Ewert, GM Gallina, GJS Bluth, and GL Swanson. Volcanic-ash hazard to aviation during the 2003-2004 eruptive activity of anatahan volcano, commonwealth of the northern mariana islands. *Journal of Volcanology and Geothermal Research*, 146(1):241–255, 2005.

[8] M Guffanti, GC Mayberry, TJ Casadevall, and R Wunderman. Volcanic hazards to airports. *Natural Hazards*, 51(2):287–302, 2009.

[9] P Sammonds, W McGuire, and S Edwards. Volcanic hazard from iceland: Analysis and implications of the eyjafjallajokull eruption. 2010.

[10] DH Landers, SM Simonich, D Jaffe, L Geiser, DH Campbell, A Schwindt, C Schreck, M Kent, W Hafner, and HE Taylor. The western airborne contaminant assessment project (wacap): An interdisciplinary evaluation of the impacts of airborne contaminants in western us national parks. *Environmental Science and Technology*, 44(3):855–859, 2010.

[11] CE Corrigan, GC Roberts, MV Ramana, D Kim, and V Ramanathan. Capturing vertical profiles of aerosols and black carbon over the indian ocean using autonomous unmanned aerial vehicles. *Atmospheric Chemistry and Physics*, 8(3):737–747, 2008.

[12] S Higashino, M Funaki, N Hirasawa, M Hayashi, and S Nagasaki. *Development and Operational Experiences of UAVs for Scientific Research in Antarctica*, pages 159–173. Springer, 2013.

[13] VA Marple and BYH Liu. Characteristics of laminar jet impactors. *Environmental Science and Technology*, 8(7):648–654, 1974.

[14] VA Marple and K Willeke. Impactor design. *Atmospheric Environment*, 10(10):891–896, 1976.

[15] KR May. The cascade impactor: an instrument for sampling coarse aerosols. *Journal of Scientific instruments*, 22(10):187, 1945.

[16] KR May. Aerosol impaction jets. *Journal of Aerosol Science*, 6(6):403–411, 1975.

[17] GJ Newton, OG Raabe, and BV Mokler. Cascade impactor design and performance. *Journal of Aerosol Science*, 8(5):339–347, 1977.

[18] VA Marple. History of impactors-the first 110 years. *Aerosol Science and Technology*, 38(3), 2004.

[19] VA Marple, KL Rubow, and SM Behm. A microorifice uniform deposit impactor (moudi): Description, calibration, and use. *Aerosol Science and Technology*, 14(4):434–446, 1991.

[20] TA Cahill, PJ Feeney, and RA Eldred. Size-time composition profile of aerosols using the drum sampler. *Nuclear Instruments and Methods in Physics Research Section B: Beam Interactions with Materials and Atoms*, 22(1):344–348, 1987.

[21] TA Cahill and P Wakabayashi. Compositional analysis of size-segregated aerosol samples. *Advances in Chemistry Series*, 232:211–211, 1993.

[22] OG Raabe, DA Braaten, RL Axelbaum, SV Teague, and TA Cahill. Calibration studies of the drum impactor. *Journal of Aerosol Science*, 19(2):183–195, 1988.

[23] N Bukowiecki, M Hill, R Gehrig, CN Zwicky, P Lienemann, F Hegedus, G Falkenberg, E Weingartner, and U Baltensperger. Trace metals in ambient air: hourly size-segregated mass concentrations determined by synchrotron-xrf. *Environmental Science and Technology*, 39(15):5754–5762, 2005.

[24] DA Lundgren. An aerosol sampler for determination of particle concentration as a function of size and time. *Journal of the Air Pollution Control Association*, 17(4):225–229, 1967.

[25] DE Atkinson, K Sassen, M Hayashi, CF Cahill, G Shaw, D Harrigan, and H Fuelberg. Aerosol properties over interior alaska from lidar, drum impactor sampler, and opc-sonde measurements and their meteorological context during arctas-a, april 2008. *Atmospheric Chemistry and Physics*, 13(3):1293–1310, 2013.

[26] N Bukowiecki, R Gehrig, M Hill, P Lienemann, CN Zwicky, B Buchmann, E Weingartner, and U Baltensperger. Iron, manganese and copper emitted by cargo and passenger trains in zÃijrich (switzerland): size-segregated mass concentrations in ambient air. *Atmospheric Environment*, 41(4):878–889, 2007.

[27] N Bukowiecki, P Lienemann, M Hill, R Figi, A Richard, M Furger, K Rickers, G Falkenberg, Y Zhao, and SS Cliff. Real-world emission factors for antimony and

other brake wear related trace elements: size-segregated values for light and heavy duty vehicles. *Environmental Science and Technology*, 43(21):8072–8078, 2009.

[28] N Bukowiecki, P Lienemann, M Hill, M Furger, A Richard, F Amato, ASH Prevot, U Baltensperger, B Buchmann, and R Gehrig. Pm10 emission factors for non-exhaust particles generated by road traffic in an urban street canyon and along a freeway in switzerland. *Atmospheric Environment*, 44(19):2330–2340, 2010.

[29] CF Cahill, PG Rinkleff, J Dehn, PW Webley, TA Cahill, and DE Barnes. Aerosol measurements from a recent alaskan volcanic eruption: Implications for volcanic ash transport predictions. *Journal of Volcanology and Geothermal Research*, 198(1):76–80, 2010.

[30] TA Cahill, DE Barnes, and NJ Spada. Seasonal variability of ultra-fine metals downwind of a heavily traveled secondary road. *Atmospheric Environment*, 94:173–179, 2014.

[31] TA Cahill, DE Barnes, NJ Spada, JA Lawton, and TM Cahill. Very fine and ultrafine metals and ischemic heart disease in the california central valley 1: 2003-2007. *Aerosol Science and Technology*, 45(9):1123–1134, 2011.

[32] TA Cahill, DE Barnes, E Withycombe, and M Watnik. Very fine and ultrafine metals and ischemic heart disease in the california central valley 2: 1974âĂŞ1991. *Aerosol Science and Technology*, 45(9):1135–1142, 2011.

[33] TA Cahill, TM Cahill, DE Barnes, NJ Spada, and R Miller. Inorganic and organic aerosols downwind of california's roseville railyard. *Aerosol Science and Technology*, 45(9):1049–1059, 2011.

[34] Y Zhao, SS Cliff, AS Wexler, W Javed, K Perry, Y Pan, and FM Mitloehner. Measurements of size-and time-resolved elemental concentrations at a california dairy farm. *Atmospheric Environment*, 2014.

[35] A Rango and AS Laliberte. Impact of flight regulations on effective use of unmanned aircraft systems for natural resources applications. *Journal of Applied Remote Sensing*, 4(1):043539–043539, 2010.

[36] U.S. Government Accountability Office. Unmanned aircraft systems: Use in the national airspace system and the role of the department of homeland security. Statement

of Gerald L. Dillingham, Ph.D., Director, Physical Infrastructure Issues, Before the Subcommittee on Oversight, Investigations, and Management, Committee on Homeland Security, House of Representatives, July 19, 2012, GAO-12-889T.

[37] Federal Aviation Administration. Faa aerospace forecasts fy2012-2032. p. 57.

[38] RA Clothier and RA Walker. Determination and evaluation of uav safety objectives. 2006.

[39] H Chao, Y Cao, and Y Chen. Autopilots for small fixed-wing unmanned air vehicles: A survey. In *Mechatronics and Automation, 2007. ICMA 2007. International Conference on*, pages 3144–3149. IEEE, 2007.

[40] H Chao, Y Cao, and Y Chen. Autopilots for small unmanned aerial vehicles: a survey. *International Journal of Control, Automation and Systems*, 8(1):36–44, 2010.

Chapter 2
Experimental End-Station at the Stanford Synchrotron Radiation Lightsource: Development and Experimental Results[1]

Abstract

The X-ray fluorescence Induced by Polychromatic Beam end-station (XIPline, pronounced "zipline") began development and operation at the Stanford Synchrotron Radiation Lightsource (SSRL) in early 2012. The end-station is a collaboration of the University of California Davis, University of Alaska Fairbanks, and the SSRL. Since its initial development, the end-station has been used as an element specific analytical tool for a variety of environmental, metallic, and mineral samples. Presented here are the motivations for development, the specifications of the beamline end-station, and two examples of recent experiments performed. Specifically we look at analysis of an aerosol deposited substrate to demonstrate the main purpose of this line and we also show our analysis of the recent Sutter's Mill Meteorite, an example of bulk sample analysis.

[1]Published as Barberie, SR., TA. Cahill, CF. Cahill, TM. Cahill, CR. Iceman, DE. Barnes, 2013. UC Davis XIPline ("zipline") end-station at the Stanford Synchrotron Radiation Lightsource: Development and experimental results, *Nuclear Instruments and Methods in Physics Research Section A: Accelerators, Spectrometers, Detectors and Associated Equipment*, **729**.

2.1 Introduction

The XIPline end-station at the Stanford Synchrotron Radiation Lightsource (SSRL) at the Stanford Linear Accelerator Center (SLAC) is a broadly applicable tool for composition determination of material samples using Synchrotron Radiation Induced X-ray Fluorescence (S-XRF). The end-station is developed and utilized by the University of California Davis (UC Davis) DELTA Group and by scientists from Arizona State University and the University of Alaska Fairbanks's Geophysical Institute and Departments of Chemistry and Biochemistry.

Historically, the UC Davis DELTA Group's experience with similar beamlines began in 1997, when the group developed a polarized white-beam end-station based on the 18 keV bending magnet beamline 10.3.1 of the Advanced Light Source (ALS), Lawrence Berkeley National Laboratory. The development was driven by the need for S-XRF analyses over a wide range of elements for the low mass aerosol samples delivered by time- and size-resolved aerosol impactors. In the past 15 years, hundreds of quantitative multi-elemental S-XRF analyses, corresponding to tens of thousands of individual S-XRF spectra, have been used to support local, regional, and global studies in atmospheric aerosols. This research produced unprecedented sensitivities in the femtogram per cubic meter of air range for aerosols from the Greenland Summit site [1] and critical data on ultra-fine metals and health [2] [3] [4]. However, the ALS system has several deficiencies, including a low excitation energy that limits the observable elements and a restrictive geometry that does not allow analysis of non-aerosol bulk type samples. To overcome the ALS's limitations, a program was developed at the SSRL to supplement the ALS capability; building on prior experience with polychromatic beams (also known as white-light or continuum beams) and adding capabilities for monochromatic excitation at energies up to 38 keV, the XIPline end-station was developed.

The strength of the XIPline end-station is its ability to quantitatively measure the concentrations of a broad spectrum of elements simultaneously in a very short time span (approximately 10 seconds per spectrum) by a completely non-destructive process: white-beam X-ray illumination and subsequent detection of elemental fluorescence. This is done while maintaining the flexibility and adaptability to be quickly reconfigured for new analytical challenges, such as adding beam filters or employing the somewhat more "classical" approach to synchrotron XRF of using crystal monochromators for energy selection.

2.2 Station Description

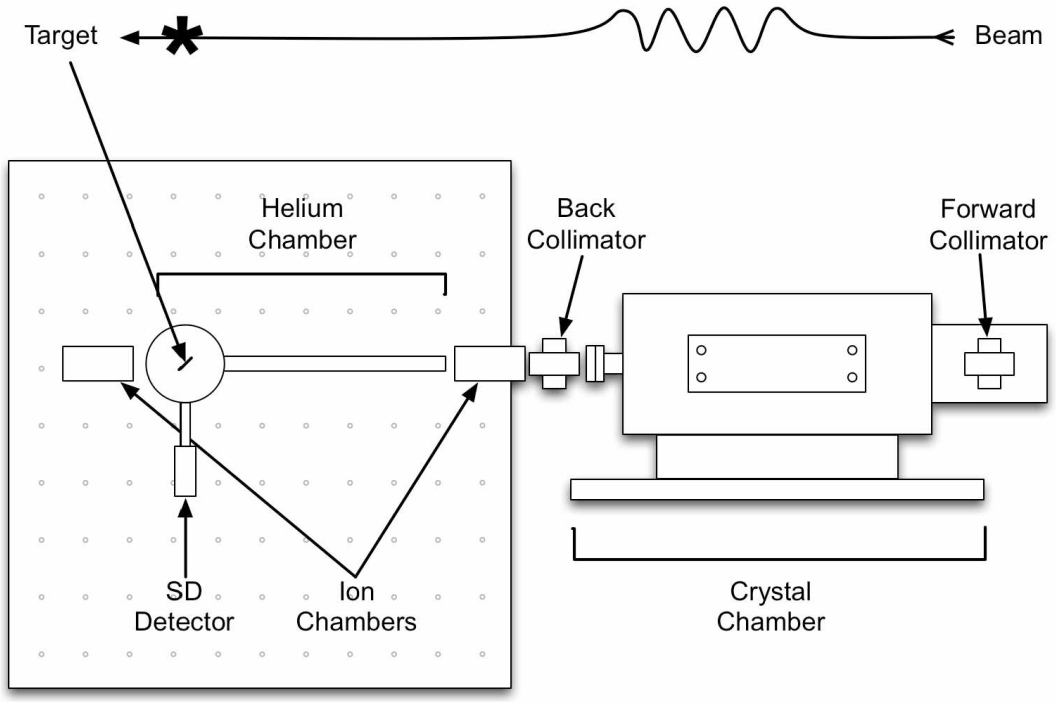

Figure 2.1. Diagram of the XIPline end-station. Polarized X-rays from the synchrotron transverse the crystal chamber with optional use of a monochromator, motorized collimators follow for adjusting the size of the beam spot. Background is reduced by simulating a vacuum with a helium chamber. The detector is placed normal to the incident beam to exploit polarization with primary scattering.

XIPline is located on beamline 2-2 at the SSRL, one of two white-light stations currently at the facility. The beamline uses radiation from a bending magnet providing a declared energy range of 1-40 keV (with an "in practice" upper-bound that can exceed 50 keV). The unaltered beam spot size is 4.0 mm $\times$ 8.0 mm. The unfiltered flux is typically on the order of 10^{10} photons per second. A simple diagram of the layout is shown in Figure 1. The beam initially comes off the synchrotron ring from the right (on the diagram) and passes through the crystal chamber where the monochromator is housed. In the case where a white-beam is desired, the crystal chamber is left empty. Motorized collimators are in the line of the beam following the crystal chamber. As the beam passes through these adjustable collimators the beam spot size is reduced as desired. The first ion chamber then measures the flux of the beam, after which the X-rays pass into the helium chamber (details below). The beam next passes through the simulated-vacuum of the helium chamber and

is incident upon the sample under analysis, the sample gives off fluorescence X-rays that are registered by the silicon drift detector. The detector itself is placed normal to and in the plane of the incident beam to take advantage of the high polarization of the synchrotron X-rays, eliminating 97.5% of the primary Compton background. The remainder of the beam that passes through the sample is then able to exit the helium chamber and pass through a second ion chamber, measuring the residual beam flux.

The sample holder and translator is encased in the helium chamber so as to provide an easy-to-access simulated vacuum that does not require the pump-down time for a true evacuated chamber. The helium chamber is a vertical-standing cylindrical acrylic enclosure that was designed and built by the UC Davis team. All windows into and out of the helium chamber are Kapton ®(DuPont). Samples are mounted in the chamber on 21 cm $\times$ 2.5 cm PTFE frames that were originally designed to simplify the analysis of the multiple aerosol samples impacted on Mylar strips utilized by DRUM samplers. The chamber translates the frame vertically using a stepper motor, allowing for the analysis of multiple samples on one frame or of time-resolved aerosol-impacted Mylar strips in half-millimeter steps, an analysis that often requires 340 half-millimeter steps to span the sample area of a standard frame i.e. 340 individual spectra. The frames are loaded into the chamber from the bottom and stepped through a small opening into the helium filled portion of the chamber. This bottom loading procedure allows frames to be changed with relatively little helium loss; however, to ensure consistency, a continuous helium flow of 0.03 cubic meters per hour is fed into the top of the chamber. Since multiple samples may be mounted on a single frame, many analyses can be performed without having to change frames; a procedure which is itself fairly quick, taking less than two or three minutes. In future deployments, and as higher sensitivities are sought out, the helium chamber may be replaced for the reduced background benefits of a true vacuum, however, this will result in a longer sample changing time.

White-beam analysis is the primary use for XIPline, hence the emphasis on polychromatic beams in the end-station name. When used as a white-beam, the monochromator chamber is left empty, allowing the beam to pass. The broad wavelength spectrum of the polychromatic beam is uniquely valuable for detection of multiple elements where sample composition is unknown. These conditions are critical when detection of trace (ppm) unexpected pollutants is of paramount importance; such as in environmental monitoring and especially so with aerosol monitoring. Impacted aerosol samples often have very little

mass, thus the intensity of the beam coupled with the low background benefits of polarization make white-beam XRF well suited to aerosol studies; additional discussion of which appears in the aerosol case study of section 3.1.

For detection of elemental fluorescence, an SII Vortex silicon drift diode (SDD) detector (Vortex EX, SII Nano Technology USA) is used. The detector was selected for its high resolution at increased count rates as well as thermoelectric cooling. The unique design of the hexagonal crystal greatly reduces the drift times as compared to standard Si(Li) detectors, permitting an order of magnitude increase in detector count-rate that is well matched to the intense X-ray flux produced by samples that are exposed to the polychromatic beam. The detector's resolution allows for well-defined peaks that ease the process of spectrum de-convolution. The high detector count-rate results in reduced experimental dead-times, which are crucial for white-beam sample excitation; since the intensity of the white-beam can often result in prohibitively high dead-times. The reduction in dead-time also shows benefits when analyzing bulk samples, since they can also produce a high flux of fluorescence X-rays. Additional details of the SDD detector can be found in [5] [6].

For peak identification and spectrum fitting we make use of a combination of in-house spectrum processing toolkits and some more established software suites, specifically Canberra's WinAXIL (Canberra, Meriden, CT, USA) and the European Synchrotron Radiation Facility's (ESRF) PyMca [7].

Although the end-station is largely focused on applications of white-beam XRF, three monochromators are also readily available for use when specific purposes require: a Si(1 1 1) monochromator with a peak acceptance at around 2.5 keV and a sharp falloff up to around 20 keV; a Si(2 2 0) crystal, corresponding to a peak at around 4 keV and falling off until around 40 keV; and lastly a Si(4 0 0) monochromator with peak acceptance around 7 keV and a sharp falloff that concludes near 50 keV. The particular uses and strengths of these respective crystals for use with synchrotron radiation are well established in the literature [8]; some additional considerations, however, will be addressed in a future methods paper that will provide a cookbook approach to S-XRF analysis for a variety of sample types. Recently the Si(4 0 0) crystal has been utilized in non-destructive testing of the Sutter's Mill meteorite [9], to be presented as a case study in Section 3.2.

2.3 Examples of Recent Studies Performed at XIPline

The primary goal of the end-station is to perform non-destructive composition analysis by means of S-XRF on samples that are traditionally difficult to measure or on unique samples that must not incur any harm during the process. Provided in this section are two such examples, the first of the former type and the second of the latter.

2.3.1 Aerosol Studies

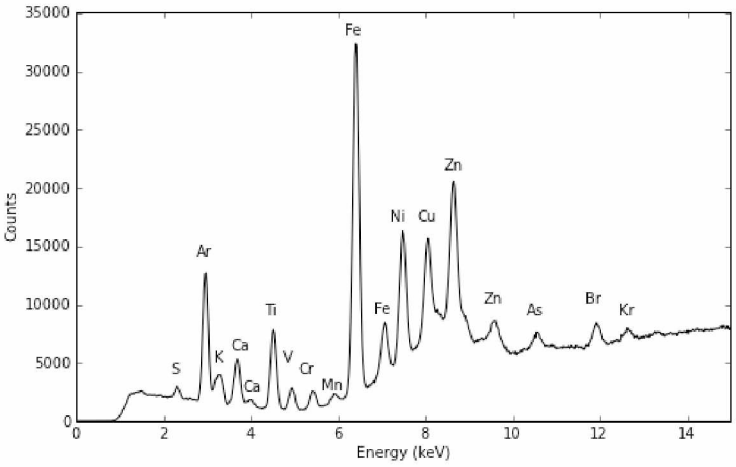

Figure 2.2. Example spectrum from S-XRF of an aerosol sample. This particular sample was collected downwind of a California rail yard. The goal of the study was to determine the concentrations and elemental composition of particulate matter emissions from the facility. As is shown in the figure, the target elements for this study were primarily the transition metals.

XIPline has been used extensively for analysis of impacted aerosol samples from air quality and pollution monitoring, an area of study where size and time resolution is often sacrificed to collect greater sample mass necessary for conventional characterization techniques. The high flux beam and XIPline's ability to run in either polychromatic or selectively filtered modes eliminate the low-signal issues from small mass deposition. A DRUM aerosol sampler [10] [11] is used at remote sites to impact particulate matter onto Mylar substrates. These substrates are then taken to XIPline and analyzed for composition. For illustrative purposes, the spectrum of one such impacted aerosol sample is shown in Figure 2. The sample in Figure 2 was collected downwind of a railroad repair depot to determine the concentrations of particulate metals emitted from the facility. The quantitative

results of the study can be found in [4].

Samples of this type, extended Mylar strips of impacted particulate matter, are best analyzed with a white-beam for the broad range of elements that the sample deposition will provide. As previously mentioned, white-beam analysis is advantageous for aerosol samples because of the abundant counts provided by the high-intensity continuum beam; since without such intensity, accumulating sufficient signal to noise resolution on elemental peaks from such low-mass samples can be prohibitively difficult. Although the K-lines for the elements of interest were all below 15 keV in the example spectrum (Figure 2) and could have conceivably been observed with a monochromator, the reduced intensity brought about by monochromatic excitation coupled with the low mass of the sample would have resulted in reduced sensitivity. Additionally, there is some room for procedural variation depending on whether trace-element (ppm) sensitivity is being limited by spectrum dominating low-energy peaks, where selective filtering may help isolate a particular energy-range of the spectrum.

In those cases, we will often start with a white-beam for our initial observations of the sample. If it is discovered that soft X-ray peaks are dominating the spectrum, filters are added to suppress the lower energy peaks and give resolution to the upper portion of the spectrum. Thus, although the polychromatic beam is often the best choice for low mass samples like aerosols, the process can be a balancing act between the white-beam and a high-pass beam created by using filters to suppress soft X-rays.

For quantitative analysis, thin-film standards are analyzed using the same experimental conditions as the samples. From these standards, the end-station yield as a function of X-ray energy can be generated for the configuration being used. For quality assurance, standards are run both before and after the samples of interest. This comparator method for quantitative analysis does require additional time, however, the short spectrum collection time (about 10 seconds per spectrum) is not prohibitive.

2.3.2 Meteorites

In another recent study, the XIPline end-station was used as a component of the global collaboration to analyze the meteorite fragment Sutter's Mill 51 (SM51) [9]. The sample analyzed had been cut to expose a flat surface which was exposed to a 1 mm $\times$ 1 mm beam of monochromatic 38 keV polarized X-rays obtained using the Si(4 0 0) monochromator crystal. The Si(4 0 0) was selected to allow a broad range of elemental detection

Table 2.1. Shown here is a selection of elements from the SM51 and MUR comparison. The raw-count comparison was used to derive an energy yield-curve for the SM51 sample using established MUR values. The Ratio column shows the raw counts of SM51 over the raw counts of MUR; revealing a strong similarity between the two samples.

Element	SM51	Uncertainty	MUR	Uncertainty	Ratio
Si	2527	155	2507	153	1.01
P	879	123	841	121	1.05
S	296	128	290	126	1.02
K	878	172	895	168	0.98
Ca	4772	172	4543	167	1.05
Ti	430	122	425	119	1.01
Cr	7549	607	7749	745	0.97
Mn	5895	224	5690	223	1.04
Fe	1070575	1499	1028801	1517	1.04
Co	16067	252	15375	245	1.04
Ni	55359	260	53140	249	1.04
Cu	1475	99	1420	94	1.04
Zn	1501	69	1442	65	1.04
Sr	636	56	601	51	1.06
Pd	390	50	374	46	1.04
Ag	875	58	833	54	1.05
Sb	126	93	119	82	1.06
Te	259	132	227	118	1.14
Ta	359	134	330	127	1.09
Pb	1556	278	1323	434	1.18

while reducing the beam to a sufficiently low intensity that the SM51 would not incur any damage. Additionally, the reduced intensity of the beam coming off of the silicon crystal created a lower fluorescence yield upon exciting SM51 than would be created with a white-beam configuration. This is important because bulk samples of this type often generate so many fluorescence X-rays under a white-beam configuration that the detector dead-time can reach prohibitively high levels. For quality assurance, repeat measurements were made to establish precision; after which the beam was moved in mm steps and separate measurements were taken to account for inhomogeneity in the sample.

The meteorite fragment presented a unique challenge for quantitative X-ray analysis because of its complex matrix and range of elements, presenting multiple opportunities for self-absorption effects. Ideally, we needed a standard reference material with a similar

Table 2.2. Presented here is a comparison for select elements of three of the quantification techniques used on SM51: S-XRF, table-top XRF, and ICP-MS. There was general quantitative agreement between S-XRF and the other analytical methods for elements observed in common. There were also several elements observed by S-XRF that could not be detected by the other techniques. A complete presentation of results is available in [9].

Element	Quantification	S-XRF	XRF	ICP-MS
Fe	% Mass	22.2	22.78	22.37
Si	% Mass	13.45	13.72	
S	% Mass	3.14	2.77	3.16
Ni	% Mass	1.28	1.29	1.24
Cr	% Mass	0.32	0.34	0.31
Mn	% Mass	0.17	0.19	0.18
P	% Mass	0.11	0.13	
Ti	% Mass	0.056	0.07	0.07
Ta	ppm	0.02		0.021
In	ppm	0.05		0.062
Tl	ppm	0.09		0.096
Cs	ppm	0.13		0.14
Sb	ppm	0.14		0.12
Pd	ppm	0.66		0.86
Te	ppm	1.5		1.42
Pb	ppm	1.88		1.61
Y	ppm	2.1		2.42
Sr	ppm	10.6		10.88

composition and matrix to which we could compare. Such a reference material presented itself in the form of the well-determined Murchison meteorite fragment (MUR) [12], a carbonaceous chondrite meteorite that fell in 1969 and was recovered near Murchison, Victoria in Australia. This fragment had been thoroughly analyzed by a number of techniques, making it a candidate for use as a suitable reference material for our analysis of SM51. We expected some similarity in the spectra of the two meteorites, since they were of the same type, but when we analyzed the two samples under the same beam configuration, they were far more similar than we expected. The two meteorite fragments presented not only the same range of elements but also nearly identical relative abundances of elements–all agreeing to within a few percent. The direct comparison between the two is shown in Table 1.

Based on the agreement between the two spectra, we applied the accepted literature

values for elemental composition to our Murchison spectra, providing the elemental yield of our beam configuration for that matrix type, just as we would with a laboratory provided standard. We then used this yield to analyze our SM51 spectra quantitatively. Of the elements observed in common, the analysis showed extremely good quantitative agreement, typically a few percent with the results of three groups using versions of Inductively Coupled Plasma Mass Spectrometry (ICP-MS). The comparison of analytical results from the various techniques are shown in Table 2.

2.4 Discussion

2.4.1 Comparison with Other Analytical Methods

In the Sutter's Mill case study (section 3.2), a comparison with other methods of analysis for a bulk sample was shown. These results show quantitative agreement with both traditional tabletop XRF and ICP-MS. Additionally, it can be seen that S-XRF was able to see a suite of elements not available by tabletop XRF and a few elements beyond what can be measured with ICP-MS. Although not explicitly displayed in the above table, it is important to note that ICP-MS often detects elements that are outside the observational range of XIPline, suggesting that the techniques may be complementary, depending on the target elements and the nature of the sample. In the case of aerosol samples, a complete range of elements and minimum detectable limits has not yet been determined to the satisfaction of the experimenters since the end-station is still under development and detection capabilities are expected to see further improvement.

2.4.2 Similar End-Stations

Excepting the related beamline at ALS, the XIPline's emphasis on aerosol composition analysis by polychromatic beam is relatively unique. However, XIPline is not the only white-light end-station using XRF. Noteworthy examples of other polychromatic analytical stations are found at HASYLAB (Hamburg Synchrotron Laboratory Germany) and at NSLS (National Synchrotron Light Source, Brookhaven National Laboratories, NY, USA).

2.4.3 Availability

Analysis at the XIPline end-station is available through collaboration with the UC Davis DELTA Group, as was the case with the Sutter's Mill meteorite fragment, or through col-

laboration with the affiliated scientists from the University of Alaska Fairbanks and Arizona State University. Such collaborations for the analyses of unique samples may become increasingly relevant as the end-station continues to receive upgrades and new developments for expanded capabilities.

2.5 Conclusions

We presented the XIPline end-station at the Stanford Synchrotron Radiation Lightsource, a collaboration of the UC Davis DELTA Group, the UA Fairbanks Geophysical Institute and Department of Chemistry, and the SSRL. We introduced a cross section of recent experiments already conducted at XIPline to provide some insight into the analytical range of the end-station. The XIPline end-station continues to receive upgrades and innovations for fast, high-sensitivity, highly-quantitative, non-destructive testing of an extremely broad range of materials.

2.6 Acknowledgements

We acknowledge the support of the SSRL via grant # 3626, as well as the exceptional efforts of the SSRL staff in both operational support and scientific guidance. The development of the enhanced beamline capabilities at SSRL Beamline 2-2 have been supported through a Cooperative Agreement with the Army Research Laboratory (W911NF-12-2-0068). Gratitude is extended to our two reviewers for their thoughtful comments as well as to Nicholas Spada for his valuable input on the manuscript. We would also like to thank the ESRF development team who designed and allowed open access to the PyMca elemental analysis software package.

2.7 References

[1] RA VanCuren, T Cahill, J Burkhart, D Barnes, Y Zhao, K Perry, S Cliff, and J McConnell. Aerosols and their sources at summit greenland-first results of continuous size-and time-resolved sampling. *Atmospheric Environment*, 52:82–97, 2012.

[2] TA Cahill, DE Barnes, NJ Spada, JA Lawton, and TM Cahill. Very fine and ultrafine metals and ischemic heart disease in the california central valley 1: 2003-2007. *Aerosol Science and Technology*, 45(9):1123–1134, 2011.

[3] TA Cahill, DE Barnes, E Withycombe, and M Watnik. Very fine and ultrafine metals

and ischemic heart disease in the california central valley 2: 1974-1991. *Aerosol Science and Technology*, 45(9):1135–1142, 2011.

[4] TA Cahill, TM Cahill, DE Barnes, NJ Spada, and R Miller. Inorganic and organic aerosols downwind of california's roseville railyard. *Aerosol Science and Technology*, 45(9):1049–1059, 2011.

[5] S Barkan, JS Iwanczyk, BE Patt, L Feng, CR Tull, and G Vilkelis. Vortex-a new high performance silicon drift detector for xrd and xrf applications. *Advances in X-Ray Analysis*, 46:332–337, 2003.

[6] DA Walko, DA Arms, A Miceli, and AL Kastengren. Empirical dead-time corrections for energy-resolving detectors at synchrotron sources. *Nuclear Instruments and Methods in Physics Research Section A: Accelerators, Spectrometers, Detectors and Associated Equipment*, 649(1):81–83, 2011.

[7] VA Solé, E Papillon, M Cotte, Ph Walter, and J Susini. A multiplatform code for the analysis of energy-dispersive x-ray fluorescence spectra. *Spectrochimica Acta Part B: Atomic Spectroscopy*, 62(1):63–68, 2007.

[8] R Van Grieken and A Markowicz. *Handbook of X-Ray Spectrometry*. CRC Press, 2001.

[9] P Jenniskens, MD Fries, QZ Yin, M Zolensky, AN Krot, SA Sandford, D Sears, R Beauford, DS Ebel, and JM Friedrich. Radar-enabled recovery of the sutter's mill meteorite, a carbonaceous chondrite regolith breccia. *Science*, 338(6114):1583–1587, 2012.

[10] TA Cahill, PJ Feeney, and RA Eldred. Size-time composition profile of aerosols using the drum sampler. *Nuclear Instruments and Methods in Physics Research Section B: Beam Interactions with Materials and Atoms*, 22(1):344–348, 1987.

[11] OG Raabe, DA Braaten, RL Axelbaum, SV Teague, and TA Cahill. Calibration studies of the drum impactor. *Journal of Aerosol Science*, 19(2):183–195, 1988.

[12] K Kvenvolden, J Lawless, K Pering, E Peterson, J Flores, C Ponnamperuma, IR Kaplan, and C Moore. Evidence for extraterrestrial amino-acids and hydrocarbons in the murchison meteorite. 1970.

Chapter 3

Evaluation of Different Synchrotron Beam Line Configurations for X-ray Fluorescence Analysis of Environmental Samples[1]

Abstract

Synchrotron Radiation X-Ray Fluorescence (SR-XRF) is a powerful elemental analysis tool, yet synchrotrons are large, multi-user facilities that are generally not amenable to modification. However, the x-ray beam lines from the synchrotrons can be modified by simply including x-ray filters or removing monochromators to improve the SR-XRF analysis. In this study, we evaluated four easily applied beam line configurations for the analysis of three representative environmental samples, namely a thin aerosol sample, an intermediate thickness biological sample, and a thick rare earth mineral specimen. The results showed that the white beam configuration, which is simply the full, polychromatic output of the synchrotron, was the optimal configuration for the analysis of thin samples with little mass. The filtered white beam configuration removed the lower energy x-rays from the excitation beam and hence it gave better sensitivity for elements emitting more energetic x-rays. The filtered white beam - filtered detector configuration sacrifices the lower energy part of the spectrum (<15 keV) for improved sensitivity in the higher end ($\approx$ 26 to 48 keV range). The use of a monochromatic beam, which tends to be the standard mode of operation for most SR-XRF analyses reported in the literature, gave the least sensitive analysis.

[1]Published as Barberie, SR., CR. Iceman, CF. Cahill, TM. Cahill, 2014. Evaluation of Different Synchrotron Beam Line Configurations for X-ray Fluorescence Analysis of Environmental Samples, *Analytical Chemistry.*, **86**(16).

3.1 Introduction

The trace elemental analysis of materials by x-ray methodologies, such as x-ray fluorescence (XRF), is a widespread and mature field [1] [2]. The XRF methods have three primary advantages. The first advantage is that the analysis is non-destructive so it can be applied to historical or rare artifacts that must not be damaged [3] [4] [5] [6] [7] [8]. The second main advantage of the XRF methods is that they can be conducted at microscopic scales, termed μ-XRF, to map the elemental composition of a sample with a spatial resolution of 10 μm or less [9] [10] [11] [12] [13] [14] [15] [16]. Lastly, XRF methods can be applied directly to samples without digestion which has resulted in a number of commercially available portable XRF units that can be used to determine elemental composition of samples in the field (e.g. [17]). The main limitations of XRF methods are that they typically lack the sensitivity of Inductively-Coupled Plasma Mass Spectrometry (ICP-MS) and thick samples have x-ray self absorption problems that make quantification more difficult. Synchrotron Radiation XRF (SR-XRF) increased dramatically in recent years [18] [19] [20] [21] as a means to conduct highly sensitive elemental analyses; some important aspects of which have been recently reviewed in the literature [22]. The SR-XRF has an intense, polarized x-ray beam that, with proper location of the detector in the plane of polarization, lowers the background in the spectra by an order of magnitude or more, hence improving the sensitivity of the analysis. The relatively recent advances in x-ray detectors, namely the silicon drift detectors (SDD), provide considerably higher x-ray counting rates so the detectors are a natural companion to the synchrotron excitation that can provide a high degree of sample excitation. The intensity of the beam can generate enough emissions from even small samples, as in micro-mapping experiments, to provide elemental spectra. Many research groups around the world use SR-XRF for various trace element analyses, yet a discussion on the optimal conditions for different types of analyses is largely lacking in the literature. Most research groups simply use the synchrotron beam lines that are available to them because the synchrotron beam lines are large, multi-user research facilities that are not amenable to major modification by individual research groups for specific studies. The majority (e.g. [3] [4] [6] [7] [8] [9] [10] [11] [14] [15] [16] [23]) of trace element analyses take the polychromatic output from the synchrotron and pass it through a monochromator to generate a single, tunable excitation energy. The selection of a single energy for excitation provides the greatest selectivity for the analysis but it comes at a cost of greatly reduced photon intensity that limits sample excitation. Another configuration

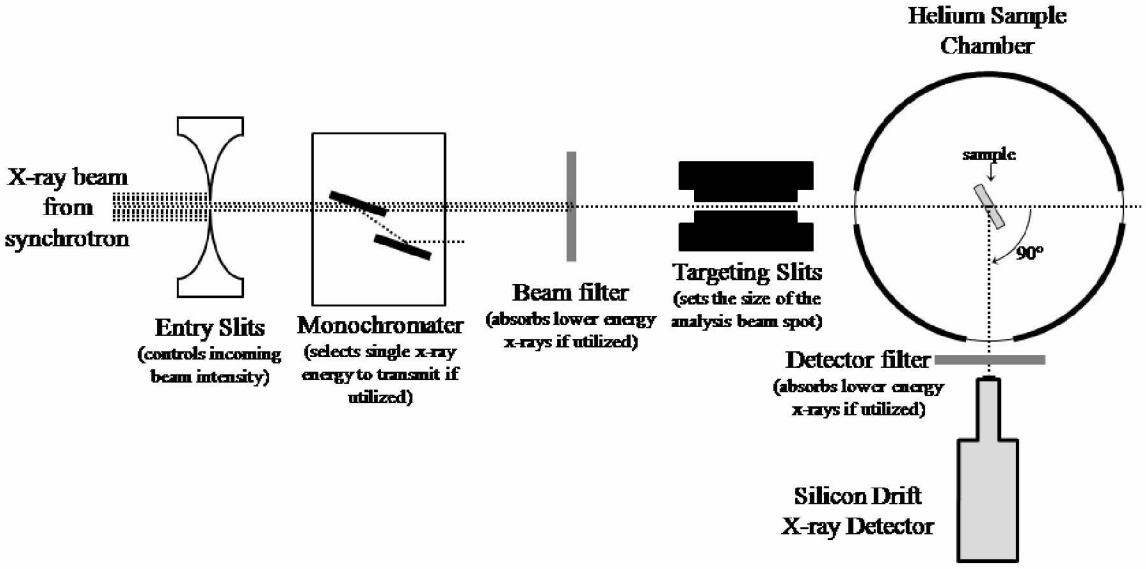

Figure 3.1. Schematic diagram of the components of SSRL beamline 2.2 utilized during this study.

is to utilize the total polarized polychromatic source beam from the synchrotron, which is often termed a white beam, to excite the sample. This provides the least selective excitation mode but the greatest photon flux that may be needed to excite small amounts of sample mass.

Very few research groups use white beam synchrotron radiation for sample excitation. The only two groups we could locate were aerosol researchers based in California (using the Advanced Light Source beam line 10.3.1 in Berkeley) [24] [25] [26] [27] and Switzerland (using both the Swiss Light Source and HASYLAB in Hamburger, Germany) [28] [29] [30] [31] [32] that employ similar methodologies. Both these groups were driven to white beam analyses by the small mass delivered by their use of time resolved and size segregated aerosol samplers. A potential intermediate option would be to use a primary beam filter to remove part of the polychromatic excitation energy in the region where maximum sensitivity is desired, thus lowering the background for a particular energy range of elements. The use of a primary beam filter (for example, see references [1] [33] [34]) to increase sensitivity for selected elements is a widespread technique used by x-ray tube-based systems since the 1960s [35], but it has been rarely utilized, or rarely reported, by the synchrotron research groups conducting elemental analyses [28] [31]. The objective of this study was to evaluate the performance of four different synchrotron beam line configurations for the

elemental analysis of three typical environmental samples. The beam line configurations were all options that are typically available to users with minimal or no beam line modifications. The beam line configurations investigated were 1) a white beam, which was the total, polychromatic x-ray emissions from the synchrotron, 2) a filtered white beam, 3) a filtered white beam and a filtered detector and 4) a monochromatic x-ray beam generated by a Si(400) crystal. These beam line configurations were tested on a set of three typical environmental samples to determine which configuration was optimal for each type of sample. The environmental samples were chosen to represent different thicknesses of sample substrates typically analyzed by XRF. The samples selected for this evaluation study were a thin aerosol sample, an intermediate thickness biological sample and a thick rare earth mineral specimen.

3.2 Experimental Section

The optimization of SR-XRF was conducted at the Stanford Synchrotron Radiation Lightsource (SSRL) at the SLAC National Accelerator Laboratory (SLAC). This instrument is a 3 GeV synchrotron that typically operates at a current of 450 to 500 mA. Beam line 2-2 was chosen for this study since it has the highest energy x-rays of any of the beam lines at SSRL; it is also one of only two polychromatic-ready beamlines at the facility. This beam is derived from a bending magnet. The median x-ray energy for this beam line was approximately 20 keV and the majority of the photon flux is below 40 keV. However, some photon flux as high as 55 keV was present. For experimenters wishing to use this method, when submitting a proposal to a synchrotron user facility and selecting a desired beam line, we recommend that the experimenter first discover which beam lines are amenable to unobstructed polychromatic excitation, and then among those, select the line with the highest energy; since the range of elements that can be detected with SR-XRF is a function of the maximum excitation energy of the beam. It was by this method that we selected beam line 2-2 for our study.

The experimental platform inside the hutch consisted of several components as shown in Figure 1 to control and modify the x-ray beam from the synchrotron. Prior to entering the hutch, the beam was passed through a set of entry slits that decrease the intensity of the beam delivered to the hutch. The maximum beam intensity was obtained when these slits are fully open. The incoming beam intensity was often decreased at this point to avoid excessive sample excitation that might saturate the x-ray detector. The next beam

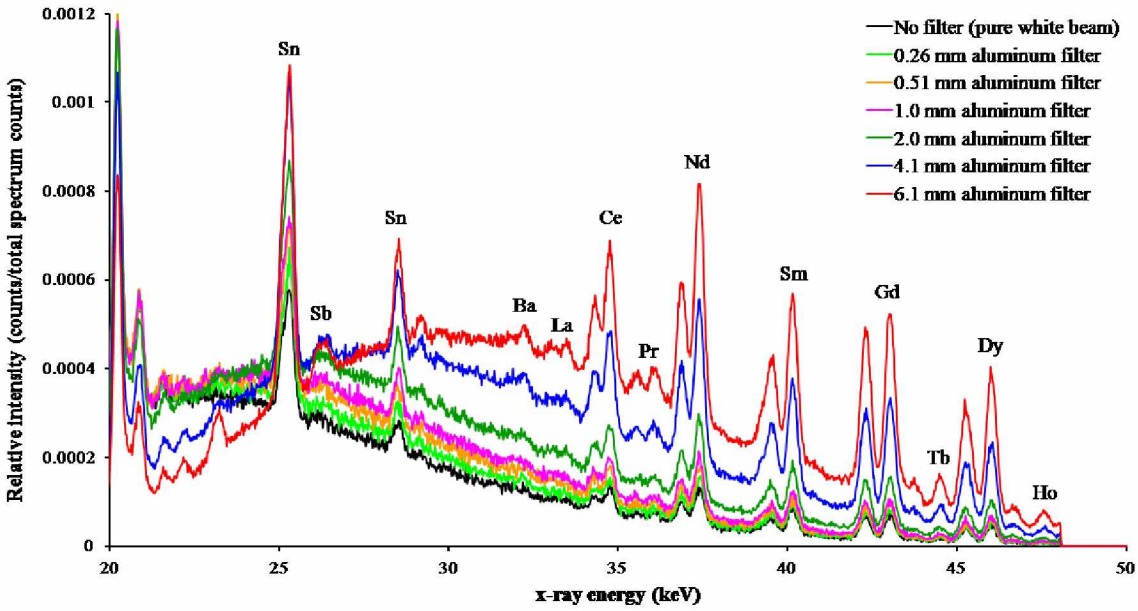

Figure 3.2. Optimization of the thickness of aluminum beam filter for the analysis of rare earth elements in a mineral sample of aeschynite-(Y). These analyses were conducted using a 2 mm aluminum detector filter. Both the 4.1 and 6.1 aluminum beam filters were able to detect more elements that the thinner beam filters. However, the 6.1 mm filter reduced the beam intensity too much for the analysis of thinner samples, hence the 4.1 mm filter thickness was chosen as the optimal thickness for the range of samples investigated in this study. The 4.1 mm aluminum filter was made by folding a sheet of regular Reynolds Wrap aluminum foil (98.5% pure aluminum with iron and silicon making up the remaining 1.5%) eight times to give 256 layers of aluminum foil.

control device (if utilized) was a monochromator that can transmit a single photon energy down the beam line. This monochromator employed a Si(400) crystal with a lattice spacing (or d-space) of 1.357755 Å that tends to perform well with higher energy x-rays. For this study, the monochromator was set to 38 keV so that maximum sensitivity would be achieved for elements with x-ray energies between 15 and 28 keV (or about Zr to Te, Th and U). Additionally, the 38 keV beam energy resulted in the incoherent Compton peak falling in the relatively unimportant part of the spectrum near the Kα1 line of xenon. Since the monochromator transmits only a single x-ray energy from all of the energies available in the incident beam, the intensity of the transmitted beam was greatly decreased so the entry slits are typically completely open to deliver the maximum x-ray intensity. The next beam control device (if utilized) was a beam filter, the composition and thickness of which were optimized during this study. The beam filter was never used in conjunction with the monochromator; the beam filter and monochromator represent two different ways to modify the incoming x-ray beam. Four different metal foils (aluminum, zinc, molybdenum and silver and six different thicknesses of aluminum filters were tested, the results of which are shown in Table 1 and Figure 2, respectively. Ultimately, a 4.1 mm thick aluminum filter was selected as the optimal filter for this beam line and application. The beam filter absorbed a large fraction of the lower energy x-rays from the incoming x-ray beam while transmitting most of the higher energy x-rays. This resulted in an excitation beam with a greater proportion of the higher energy x-rays. This also lowered the background caused by Compton scattering in the part of the spectrum where the energy was absorbed. The beam filter decreases the intensity of the transmitted x-ray beam, but the decrease of beam intensity was not as large as from the monochromator. The principle of filtering of polychromatic x-ray sources to provide improved sensitivity for certain parts of the spectra is well established [1] [33] [34] [35] and is used by some commercially available bench-top XRF systems. However, it is very rarely reported in SR-XRF analyses [28] [31] and never discussed in great detail. If neither the monochromator nor the beam filter are utilized, then a white beam was transmitted down the beam line. This was simply the full spectrum (i.e. polychromatic spectrum) of x-rays generated by the synchrotron, nominally 4 to 40 keV. The white beam had the greatest transmitted flux, but it was the least selective in terms of x-ray energies transmitted. The next stage of the beam line was the beam control slits that control the size of the beam spot (or sampling area). For this study, the beam spot was 1.0 mm $\times$ 0.5 mm unless otherwise noted, but this value can be set from anywhere

between about 0.5 mm $\times$ 0.5 mm to 6 mm $\times$ 2 mm. Larger beam spots sample more area (and sample mass) and thus generate more x-ray emissions. Smaller spots are preferred for samples with spatial heterogeneity, but come at a cost of lower x-ray flux passing through the sample and hence fewer x-ray emissions from the sample. The transmitted x-ray beam passes into a helium chamber where the samples are mounted. The helium atmosphere between the samples and the x-ray detector allows for the detection of low-energy x-rays that would otherwise be absorbed by the air. The helium chamber was simply a vertically mounted acrylic cylinder that is almost completely sealed except for a small hole on the bottom that allows for sample insertion. Windows were cut into the chamber for the entry and exit of the x-ray beam as well as for the detector. The windows were then covered with a very thin layer of Kapton (DuPont) to keep the helium in the chamber but allows x-ray transmission with effectively no attenuation at the x-ray energies being used in this study. The chamber has a steady stream of helium (0.03 cubic meters per hour) going through it with the extra escaping from the hole on the bottom of the chamber where the samples were inserted. The x-rays generated by the sample then may pass through a detector filter if it was utilized. Detector filters have been used in prior studies (e.g. [23] [36] [37]) to suppress detection of abundant low-end elements. The composition and the thickness of the detector filter can be easily changed depending on the particular application to remove a particular range of the spectrum. In this study, the detector filter consisted of 2.0 mm of aluminum to absorb lower energy x-rays (below about 15 keV) before they reach the detector. This sacrifices the lower range of the spectrum to give improved sensitivity for elements with higher energy x-rays because the detector will not be overwhelmed by x-rays from common and abundant elements like iron39 and calcium26. The last part of the beam line was the SII Vortex EX x-ray detector (Hitachi High-Technologies Science America, Inc.)[38] that quantified the number and the energy of the x-rays emitted from the sample. This was a silicon drift detector that can process the higher count rates found in synchrotron applications. In this study, the detector was operated at an optimal count rate that resulted in a detector dead-time of approximately 20%. The entry slits were adjusted to deliver a beam intensity to keep the detector operating at the optimal count rate. If the entry slits were completely open and the detector was still below the optimal count rate, then it was noted in the results that maximum performance would not be obtained. The detector was mounted at 90 degrees relative to the x-ray beam to take the maximum advantage of the polarized nature of the x-ray beam. However, this detector angle makes

it more likely that diffraction peaks may appear in the spectra of crystalline mineral samples when using polychromatic excitation methods. Three environmental samples were chosen to represent different matrices that are typically analyzed by x-ray fluorescence. The first sample was a particulate air sample collected on a mylar impaction substrate with an 8-stage DRUM sampler [39] downwind of the railroad repair depot in Roseville, CA [40]. This particulate size fraction represented by this sample was the 0.09 to 0.12 μm size fraction. This sample represents a very thin sample with a relatively low amount of mass present, with a thickness on the order of 30 μm. The second environmental sample was a biological sample, namely the keratin rattle from a sidewinder rattlesnake (Crotalus cerastes). The sample was collected in a relatively rural area south of Phoenix, AZ. This sample has an intermediate thickness that may result in some of the lower-energy x-rays (e.g. sulfur) being self-absorbed by the sample matrix, hence some corrections need to be applied to obtain quantitative results. The last of the representative environmental samples chosen was a rare earth mineral sample, namely aeschynite-(Y) from Hittero, Norway with a reported formula of (Y, Ca, Fe, Th)(Ti, Nb)2(O, OH)6. This sample was about 2 mm thick, but this is still considered a thick target in terms of x-ray analysis, which means that many of the lighter elements (e.g. Ca and Ti) will be under-represented in the spectrum due to matrix self-absorption effects. While absolute quantification by the application of absorption corrections is possible, this type of analysis is best for qualitative or comparative results. The sample run time was 10 minutes for every analysis in this study.

3.3 Results and Discussion

The four different beam line configurations were evaluated on 1) their ability to detect a wide range of elements (Figure 3), and 2) their sensitivity of the elements that are able to be detected (Table 2). The four different configurations had strengths and weaknesses so the different configurations were optimal for different types of samples. It is important to note that higher atomic number elements including the rare earth elements are often found in much lower concentrations in samples due to their lower abundance in nature. Therefore, a case arises wherein, although high Z elements exist in a sample, the low Z elements produce such a large spectral yield, that the detector cannot register the smaller peaks at higher energies. For this reason, one focus of our optimization efforts (particularly with respect to the beam filtering) was on suppressing the lower end of the spectrum to provide additional resolution to the upper end. It is also important to note that since higher energy

x-rays have a lower interaction cross-section with matter than lower energy x-rays, adding filters to a sample will always suppress the spectrum from the low end first. Although that fence can be moved by varying filter material, and the magnitude of the suppression can be altered by varying filter thickness, the low end of the spectrum is the only possible target for filtering. Overall, the white beam configuration provided good results over a wide range of elements as evidenced in that it was able to detect 11 elements in the aerosol sample, 21 in the rattlesnake tail and 19 in the mineral specimen (Table 2). Moreover, there were no elements that were expressly excluded by this analysis. Elements from potassium to holmium could be detected with the K line x-rays and elements from erbium to uranium could be detected with the L line x-rays. The sensitivity of the analysis, as measured by the signal-to-noise ratios, was frequently better than the other configurations with the white beam being the most sensitive in 8 of the 15 elements detected in the aerosol sample and 11 of 22 elements detected in the rattlesnake tail. Surprisingly, the white beam was the best for only one element in the mineral sample. The white beam tended to be the best for elements with lower energy x-rays (e.g. 12 keV or lower) since the white beam has more low energy x-rays to excite these elements. The white beam analyses were particularly effective for samples with very low masses, such as aerosol samples or microprobe analyses, that require a high photon flux to generate enough emissions for a sensitive spectrum. It is worth noting that the only two research groups we could find that utilized white beam analyses were primarily conducting aerosol analysis where amounts of material analyzed are very small [26] [28].

The limitations of the white beam are relatively few. In thick samples, the white beam system tended to have high count rates from common elements (e.g. iron) that limited the sensitivity for rarer elements (e.g. antimony). Furthermore, the presence of intense emission lines from abundant elements increases the occurrence of sum peaks in the spectra (Figure 3), which are the result of two low energy x-rays from an abundant element hitting the detector at the exact same time and appearing as a fictitious peak equal to the sum of their energies. In the rare earth mineral sample, a sum peak was observed in the white beam and filtered white beam analyses corresponding to the sum of two Y Kα x-rays, but the sum peak was relatively minor at 0.13% of the intensity of the Y Kα peak. Sum peaks can also be reduced by beam intensity so that the detector operates at a lower count rate (i.e. detector dead-time is reduced). The other limitation of the white beam configuration is that it is vulnerable to diffraction peaks in crystalline mineral samples. Diffraction

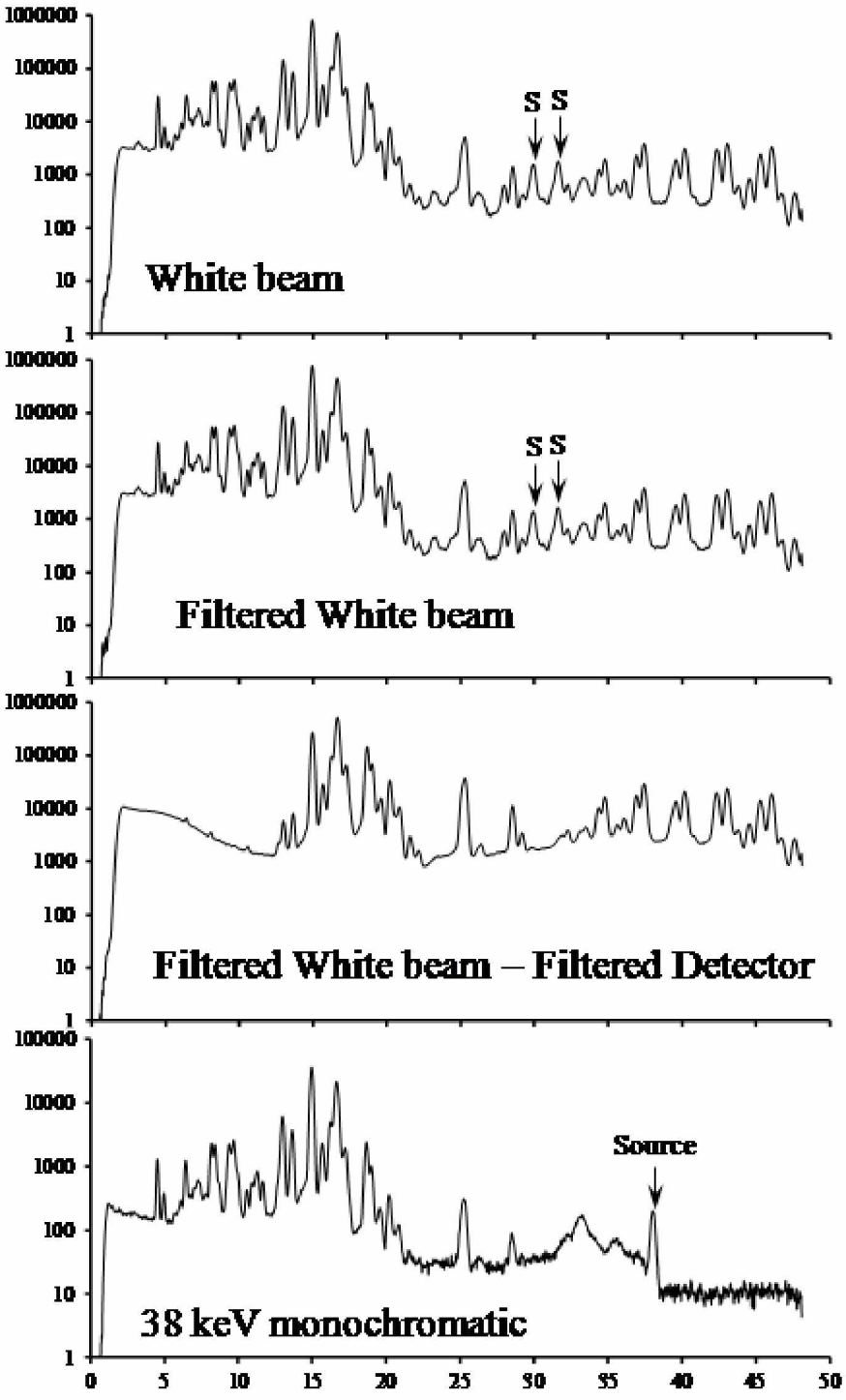

Figure 3.3. Spectra obtained from a sample of the rare earth mineral aeschynite-(Y) with the four beam line configurations investigated. Notice that the filtered white beam-filtered detector configuration cannot obtain the low end of the spectrum while the monochromatic beam cannot obtain the high end of the spectrum. The peaks labeled with an *S* and an arrow in the white beam and filtered white beam spectra are an artifact called *sum peaks* along with a few smaller peaks in that area of the spectrum. Notice that the sum peaks are absent from the filtered white beam-filtered detector and the monochromatic spectra.

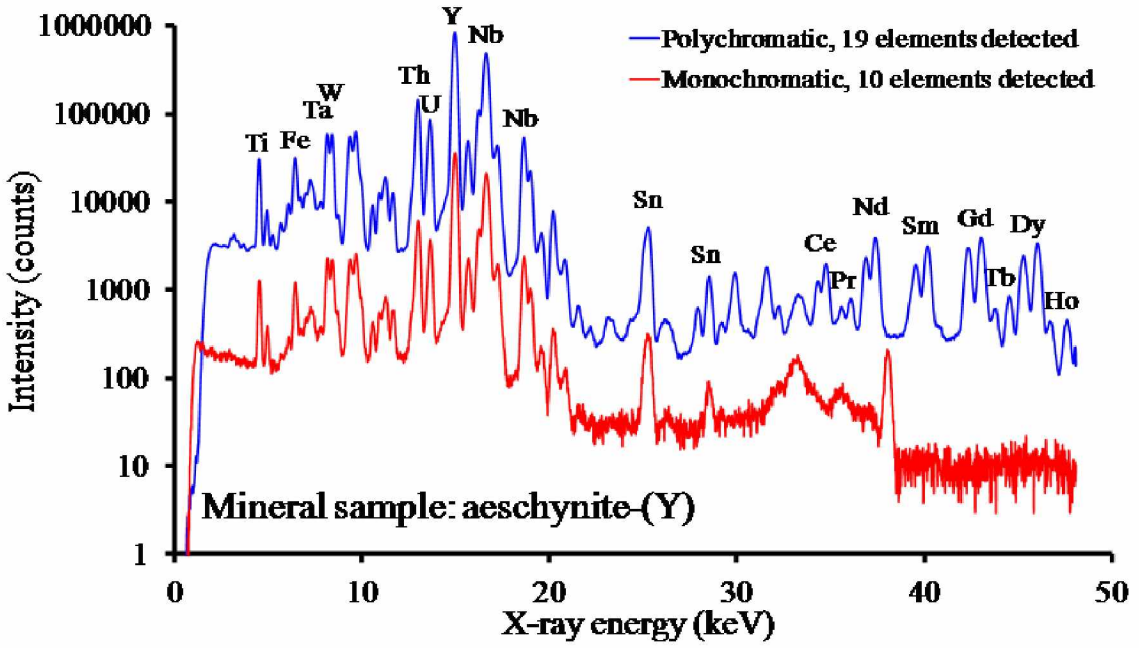

Figure 3.4. Comparison of the polychromatic and monochromatic beams for mineral sample aeschynite-(Y).

peaks occur when one of the many wavelengths of incoming source x-ray matches a wavelength that can diffract off of a crystalline material. This causes a coherent beam of source x-rays at a particular energy to strike the detector which gives a peak in the energy spectrum (see Figure S2 in supporting materials for an example). These diffraction peaks can complicate the data interpretation since they can masquerade as elemental emission peaks. While no diffraction peaks were observed in the samples analyzed in this experiment, they have been observed in other mineral samples analyzed by our group with the white beam. Diffraction peaks can be reduced or eliminated by powdering crystalline samples and using a larger beam spot to integrate over a larger area. The filtered white beam performed better than the white beam for elements with x-ray energies between 11 and 26 keV, which roughly corresponds to bromine to antimony. In the aerosol sample, the filtered white beam performed best for 7 of the 15 elements detected. Furthermore, it was able to detect an additional 4 elements (Sr, Mo, Ag, and Sb) that were not detected by the other beam line configurations. For the rattlesnake tail, the filtered white beam was the most sensitive for 9 elements of the 22 elements detected. The filtered white beam also performed well on the mineral sample (11 out of 23 elements detected). The filtered white beam detected more

elements in the three environmental samples than any other beam line configuration. The increased sensitivity to the higher energy elements was accomplished by two processes: 1) increasing the proportion of higher energy x-rays in the incoming beam by absorbing the lower energy photons and 2) lowering the background of Compton x-rays in regions of the spectra with elements of interest. The filtered white beam configuration performed the best with thicker samples (e.g. biological and mineral specimens).

The filtered white beam - filtered detector configuration was designed to increase the sensitivity of the system for the elements with the highest x-ray energies by placing a filter over the detector to eliminate the lower energy x-rays from abundant elements like calcium and iron [26] [36]. This means all of the x-rays counted by the detector originate from the higher end of the energy spectrum. However, the addition of the detector filter forsakes the lower end of the spectrum with many interesting and toxic elements. The filtered white beam - filtered detector performed poorly for the aerosol and rattlesnake samples that were dominated by elements in the lower end of the spectrum. The aerosol sample was unable to achieve anywhere near optimal detector count rate even at maximum synchrotron beam intensity, hence the data was not collected. For the rattlesnake tail, this configuration was the best for a single element, namely barium, out of the 22 elements detected. However, the filtered white beam - filtered detector was very effective at analyzing the rare earth mineral specimen since this configuration was the most sensitive for 12 elements with x-ray energies between 26 and 47 keV (or about antimony to holmium). Unfortunately, the configuration used in this study effectively sacrifices all elements with x-ray energies below about 15 keV, which encompasses most of the common elements normally detected by XRF. One fringe benefit of excluding the abundant low-energy elemental emissions is that it dramatically reduces the presence of sum peaks higher in the spectrum that might interfere with the detection of trace amounts of elements (Figure 3). Overall, the filtered beam - filtered detector is a more specialized configuration for the analysis of more energetic elements. The monochromatic beam performed poorly compared to the other beam configurations. Simply, the lower photon flux resulting from transmitting a single frequency of light was not able to generate enough x-rays from the samples to operate the detector at efficient count rate. The beam spot size in the monochromatic analyses was even increased to 6 mm $\times$ 2 mm, compared to the 1 mm $\times$ 0.5 mm of the other analyses, to compensate for the lower photon flux. Even under these large beam spot conditions, the monochromatic beam was always the least sensitive configuration

Table 3.1. Performance of the different beam filter materials on the ability of the SR-XRF system to detect elements in a rare earth mineral sample, namely aeschynite-(Y). The values represented in the table are the signal-to-noise ratios for the elements detected. The elements are listed in increasing order of their x-ray energies and the particular x-ray emission line used for the sensitivity assessment is given in parenthesis. All tests were conducted with a detector filter consisting of 2 mm of aluminum. The best beam filter for a particular element is shown in larger, bold text.

	beam filter material			
	aluminum	zinc	molybdenum	silver[b]
beam filter thickness (mm)	4.1	0.62	0.25	0.50
beam filter areal density (g/cm^2)	1.1	0.44	0.32	0.36
total spectrum counts	2.8×10^7	2.1×10^7	1.8×10^7	5.7×10^6
Y ($K_{\alpha 1}$)	**1500**	840	1400	200
Th ($L_{\beta 1}$)	**460**[c]	**280**[c]	**210**[c]	**70**[c]
Nb ($K_{\alpha 1}$)	**2800**	1600	1800	410
U ($L_{\beta 1}$)	**340**[c]	**210**[c]	**460**[c]	**100**[c]
Ag ($K_{\alpha 1}$)	7.2	11	**12**	source[d]
Sn ($K_{\alpha 1}$)[e]	**330**	220	180	62
Sb ($K_{\alpha 1}$)	7.7	6.5	5.7	3.1
Ba ($K_{\alpha 1}$)	15	**18**	14	2.3
La ($K_{\alpha 1}$)	17	**17**	16	3.0
Ce ($K_{\alpha 1}$)	130	**180**	140	37
Pr ($K_{\alpha 1}$)	30	46	33	9.8
Nd ($K_{\alpha 1}$)	260	420	330	110
Sm ($K_{\alpha 1}$)	180	340	280	110
Gd ($K_{\alpha 1}$)	200	430	370	200
Tb ($K_{\alpha 1}$)	33	72	57	40
Dy ($K_{\alpha 1}$)	170	370	350	240
Ho ($K_{\alpha 1}$)	18	43	40	33

a. The silver foil reduced the intensity of the excitation beam to the point that the detector could was not operating at an effective count rate.

b. The peak measured may consist of overlapping x-ray emissions from two elements. This also includes peaks that are on the shoulder of another peak.

c. The emission of silver x-rays from the sample could not be quantified since there were additional silver x-rays from the fluorescence of the beam filter. The amount of fluorescence x-rays from the beam filter were remarkably small (and not even detected for the molybdenum filter).

d. The tin peak was also observed in blank spectra, so it may be the result of the detector or other nearby materials.

Table 3.2. Performance of the different beam line configurations in detecting elements in the three representative sample types. The values represented in the table are the signal-to-noise ratios for the elements detected rounded to two significant digits of accuracy. If an element cannot be detected by a configuration, then it is denoted as "—". If an element could be detected but it was not quantified in this study, then it is denoted as ND if the baseline was relatively flat or INT if there is a large, interfering peak that would obscure the element. The elements are listed in increasing order of their x-ray energies and the particular x-ray emission line used for the sensitivity assessment is given in parenthesis. The beam line configurations are abbreviated as follows: WB is white beam, FWB is filtered white beam (using a 4.1 mm Al filter), FWB-FD is filtered white beam with filtered detector (using a 4.1 mm Al filter on the beam and a 2 mm Al filter on the detector), and Mono is monochromatic beam.

	thin aerosol sample (Roseville, CA)			intermediate biological sample (rattlesnake tail, Phoenix, AZ)				thick mineral sample (Aeschynite-(Y), Hittero, Norway)			
	WB	FWB	Mono	WB	FWB	FWB-FD	Mono	WB	FWB	FWB-FD	Mono
no. of detections	11	15	4	21	22	10	9	19	23	17	10
counts	3.5×10^7	1.9×10^7	9.5×10^4	5.2×10^7	4.0×10^7	1.1×10^7	7.4×10^5	3.3×10^7	3.1×10^7	2.8×10^7	1.4×10^6
K ($K_{\alpha 1}$)	INT	INT	ND	240	170	–	ND	ND	ND	–	ND
Ca ($K_{\alpha 1}$)	59	4.5	ND	1700	1300	–	1.2	2.3	2.8	–	ND
Ti ($K_{\alpha 1}$)	200	14	INT	470	430	–	8.8	160	190	–	31
V ($K_{\alpha 1}$)	INT	ND	ND	90[b]	83[b]	–	INT	26[b]	32[b]	–	INT
Cr ($K_{\alpha 1}$)	25	4.2	ND	32	11	–	ND	ND	ND	–	ND
Mn ($K_{\alpha 1}$)	20	1.9	ND	590	460	–	ND	ND	ND	–	ND
Fe ($K_{\alpha 1}$)	1400	150	2.1	22000	17000	–	34	140	180	–	29
Ni ($K_{\alpha 1}$)	130	13	ND	62	73	–	ND	ND	INT	–	INT
Cu ($K_{\alpha 1}$)	180	33	2.6	280	270	–	1.8	INT	INT	–	INT
Ta ($L_{\alpha 1}$)	INT	INT	ND	INT	INT	–	ND	ND	360	–	55
W ($L_{\alpha 1}$)	ND	ND	ND	ND	ND	–	ND	ND	370	–	56
Zn (K_{α})	320	30	9.1	710	550	–	7.8	INT	ND	–	ND
Se ($K_{\alpha 1}$)	ND	ND	ND	4.6	4.0	–	ND	INT	INT	–	INT
Br ($K_{\alpha 1}$)	19	28	ND	110	100	–	0.8	ND	ND	–	ND
Pb ($L_{\beta 1}$)	17	47	ND	21[b]	75[b]	–	ND	32[b]	62[b]	–	10
Rb ($K_{\alpha 1}$)	ND	ND	ND	120	120	3.7	ND	INT	INT	ND	ND
Sr ($K_{\alpha 1}$)	ND	11	ND	360	440	32	2.6	ND	ND	ND	ND
Y ($K_{\alpha 1}$)	ND	ND	ND	38[b]	50[b]	8.9[b]	ND	6000	8900	1500	990
Zr ($K_{\alpha 1}$)	ND	ND	ND	110[b]	160[b]	47[b]	1.9	INT	INT	INT	INT
Th ($L_{\beta 1}$)	ND	ND	ND	ND	ND	ND	ND	300	1000[b]	460[b]	120
Nb ($K_{\alpha 1}$)	ND	ND	ND	6.5	15	6.9	ND	3200	4900	2800	570
U ($L_{\beta 1}$)	ND	ND	ND	ND	ND	ND	ND	300[b]	470[b]	340[b]	51
Mo ($K_{\alpha 1}$)	ND	7.0	ND	ND	ND	ND	ND	INT	INT	INT	ND
Pd ($K_{\alpha 1}$)	ND	ND	ND	ND	ND	1.0	ND	ND	ND	ND	ND
Ag ($K_{\alpha 1}$)	ND	5.8	ND	10	13	13	ND	13	0.8	7.2	ND
Sn ($K_{\alpha 1}$)[c]	17	130	4.0	14	38	35	1.8	300	88	330	14
Sb ($K_{\alpha 1}$)	ND	7.1	ND	ND	2.2	2.3	ND	ND	ND	7.7	ND
Ba ($K_{\alpha 1}$)	ND	ND	ND	3.8	9.7	18	ND	8.7	5.6	15	ND
La ($K_{\alpha 1}$)	ND	ND	–	ND	ND	ND	–	17	8.4	17	–
Ce ($K_{\alpha 1}$)	ND	ND	–	ND	ND	ND	–	49	33	130	–
Pr ($K_{\alpha 1}$)	ND	ND	–	ND	ND	ND	–	13	7.3	30	–
Nd ($K_{\alpha 1}$)	ND	ND	–	ND	ND	ND	–	110	76	260	–
Sm ($K_{\alpha 1}$)	ND	ND	–	ND	ND	ND	–	86	56	180	–
Gd ($K_{\alpha 1}$)	ND	ND	–	ND	ND	ND	–	110	70	200	–
Tb ($K_{\alpha 1}$)	ND	ND	–	ND	ND	ND	–	9.7	10	33	–
Dy ($K_{\alpha 1}$)	ND	ND	–	ND	ND	ND	–	95	55	170	–
Ho ($K_{\alpha 1}$)	ND	ND	–	ND	ND	ND	–	11	6.5	18	–

a. The peak measured may consist of overlapping x-ray emissions from two elements. This also includes peaks that are on the shoulder of another peak.

b. The tin peak was also observed in blank spectra, so it may be the result of the detector or other nearby materials.

in terms of both signal-to-noise and the number of elements detected. Furthermore, the monochromatic beam at 38 keV was unable to excite elements with higher x-ray energies, such as the K lines of the rare earth elements. The monochromatic beam at 38 keV was especially insensitive to the elements with low x-ray energies (< 8 keV) since the absorption cross-section of these elements is low. The monochromatic beam was best suited for mineral samples where the large mass of the sample can partly offset the effect of a low photon flux, but the other beam line configurations provided considerably greater sensitivity. One inherent advantage of the monochromatic beam was that it was effectively immune to diffraction peak artifacts in the spectrum when analyzing crystalline samples. The purpose of this research was to illustrate simple methods to enhance the sensitivity of SR-XRF analyses. Almost all of the SR-XRF studies use a monochromator, yet the results show that a monochromatic source was less sensitive than other options due to the dramatic decrease in photon flux that limited the amount of sample excitation. Monochromators are essential to other synchrotron applications, such as x-ray crystallography, x-ray absorption near-edge structure (XANES), etc., hence monochromators are common on synchrotron beam lines and are probably used mainly by default. This study was conducted to evaluate alternatives to a monochromator by filtering the source x-ray beam or detector to achieve increased sensitivity in selected energy ranges in the spectrum. The results of this study indicate that dramatic increases in sensitivity can be achieved by SR-XRF by simply removing the monochromator and using a white beam. The simplest way to achieve this is to remove the crystals from the monochromator and allow the white beam to pass unmodified through the monochromator housing. The use of a white beam increases sample excitation by orders of magnitude yet the polarized nature of the x-ray beam keeps the background relatively low. Bukowiecki et al. [28] also demonstrated that a white beam was far more sensitive than a monochromatic beam for thin aerosol analysis, yet almost all other research groups still use a monochromatic beam for SR-XRF. The second option is to use a primary beam filter when using a white beam. The advantage of filters is that they are simply sheets of metal that can be place in the beam line, so they do not require any significant modification to the synchrotron facility yet they deliver enhanced sensitivity for some elements. It is recommended to place the primary beam filter as far *upstream* in the beam line as possible so that any fluorescent emissions from the filter material will have spread out before they reach the sample or the detector. The use of detector filters can dramatically increase the sensitivity of the analysis for select elements with higher energy

x-rays at the expense of the elements with lower energy x-rays. Detector filters seem to be best suited for trace analysis of samples with considerable mass whose matrix is dominated by lighter elements like calcium, iron and zinc. One advantage of detector filtering is that multiple detectors can be deployed around the sample with different degrees of detector filtering. This allows one unfiltered detector to obtain the full spectrum of elements while a second (or even third) detector may be filtered to give greater sensitivity for the elements with more energetic x-rays. Given the limitations on synchrotron beam time, a multiple detector array with some detectors filtered could provide the greatest sensitivity over a wide range of elements for the least amount of beam time. Another potential option is to employ a pierced filter, also sometimes called a *funny filter* [37], that has a small hole drilled in it to allow a small fraction of the low energy x-ray to reach the detector unimpeded while blocking the rest. This suppresses the intensity of abundant low energy elements while still obtaining a complete spectrum.

3.4 Conclusions

The vast majority of SR-XRF studies reported in the literature utilize a monochromatic beam for sample excitation. However, the results from this study and a prior one by Bukowiecki et al. [28] indicate that dramatic increases in sensitivity can be obtained by simply removing the monochromator and using the polychromatic white beam from the synchrotron for sample excitation. This is especially true when using the fast x-ray detectors like the silicon drift detectors. The advantage of this approach is that no new equipment is needed and the modifications, which generally consists of removing the crystals from the monochromator housing, are simple. Both primary white beam filters and detector filters represent ways to easily customize the analysis to focus on different parts of the energy spectrum. A multiple detector array, where one or more of the detectors are filtered, could provide the greatest sensitivity over a wide range of elements in the least amount of synchrotron beam time. The filtering methods used in this study have been used by the x-ray tube XRF operators for decades, yet they have not been widely adopted by the SR-XRF researchers even though they could increase the sensitivity or selectivity of the analysis.

3.5 Acknowledgements

Portions of this research were carried out at the Stanford Synchrotron Radiation Lightsource, a Directorate of SLAC National Accelerator Laboratory and an Office of Science User Facility operated for the U.S. Department of Energy Office of Science by Stanford University. We thank the wonderful staff at SSRL who made this research project possible. In particular, we thank Tom Hostetler and David Day for their help setting up the beam line. This Project was supported in part through a Cooperative Agreement with the Army Research Laboratory (W911NF-12-2-0068) and the University of Alaska, Fairbanks.

Supporting Information Available

Supporting information includes detailed results from the evaluation of different primary beam filter materials as well as the thickness of aluminum used for the beam filter. Lastly, an example of a spectrum containing diffraction peaks resulting from the analysis of a crystalline mineral with a white beam.

3.6 References

[1] E Marguí, GH Floor, M Hidalgo, P Kregsamer, G Román-Ross, C Streli, and I Queralt. Analytical possibilities of total reflection x-ray spectrometry (txrf) for trace selenium determination in soils. *Analytical Chemistry*, 82(18):7744–7751, 2010.

[2] K Tsuji, K Nakano, Y Takahashi, K Hayashi, and C Ro. X-ray spectrometry. *Analytical Chemistry*, 84(2):636–668, 2011.

[3] EC Geil, SA LeBlanc, DS Dale, and RE Thorne. Application of x-ray fluorescence imaging to ceramics from the american southwest. *Journal of Archaeological Science*, 40(12):4780–4784, 2013.

[4] PL Manning, NP Edwards, RA Wogelius, U Bergmann, HE Barden, PL Larson, D Schwarz-Wings, VM Egerton, D Sokaras, and RA Mori. Synchrotron-based chemical imaging reveals plumage patterns in a 150 million year old early bird. *Journal of Analytical Atomic Spectrometry*, 28(7):1024–1030, 2013.

[5] G Van der Snickt, K Janssens, J Dik, W De Nolf, F Vanmeert, J Jaroszewicz, M Cotte, G Falkenberg, and L Van der Loeff. Combined use of synchrotron radiation based micro-x-ray fluorescence, micro-x-ray diffraction, micro-x-ray absorption near-edge,

and micro-fourier transform infrared spectroscopies for revealing an alternative degradation pathway of the pigment cadmium yellow in a painting by van gogh. *Analytical Chemistry*, 84(23):10221–10228, 2012.

[6] J Dik, K Janssens, G Van Der Snickt, L Van Der Loeff, K Rickers, and M Cotte. Visualization of a lost painting by vincent van gogh using synchrotron radiation based x-ray fluorescence elemental mapping. *Analytical Chemistry*, 80(16):6436–6442, 2008.

[7] L Monico, G Van der Snickt, K Janssens, W De Nolf, C Miliani, J Dik, M Radepont, E Hendriks, M Geldof, and M Cotte. Degradation process of lead chromate in paintings by vincent van gogh studied by means of synchrotron x-ray spectromicroscopy and related methods. 2. original paint layer samples. *Analytical Chemistry*, 83(4):1224–1231, 2011.

[8] B Constantinescu, A Vasilescu, M Radtke, and U Reinholz. A study on gold and copper provenance for romanian prehistoric objects using micro-sr xrf. *Journal of Analytical Atomic Spectrometry*, 26(5):917–921, 2011.

[9] DL Howard, MD de Jonge, D Lau, D Hay, M Varcoe-Cocks, CG Ryan, R Kirkham, G Moorhead, D Paterson, and D Thurrowgood. High-definition x-ray fluorescence elemental mapping of paintings. *Analytical Chemistry*, 84(7):3278–3286, 2012.

[10] E Donner, DL Howard, MD Jonge, D Paterson, MH Cheah, R Naidu, and E Lombi. X-ray absorption and micro x-ray fluorescence spectroscopy investigation of copper and zinc speciation in biosolids. *Environmental Science and Technology*, 45(17):7249–7257, 2011.

[11] D Zimmer, J Kruse, C Baum, C Borca, M Laue, G Hause, R Meissner, and P Leinweber. Spatial distribution of arsenic and heavy metals in willow roots from a contaminated floodplain soil measured by x-ray fluorescence spectroscopy. *Science of the Total Environment*, 409(19):4094–4100, 2011.

[12] R Evens, KAC De Schamphelaere, B De Samber, G Silversmit, T Schoonjans, B Vekemans, L Balcaen, F Vanhaecke, I Szaloki, and K R. Waterborne versus dietary zinc accumulation and toxicity in daphnia magna: a synchrotron radiation based x-ray fluorescence imaging approach. *Environmental Science and Technology*, 46(2):1178–1184, 2011.

[13] S Majumdar, JR Peralta-Videa, H Castillo-Michel, J Hong, CM Rico, and JL Gardea-Torresdey. Applications of synchrotron μ-xrf to study the distribution of biologically important elements in different environmental matrices: A review. *Analytica Chimica Acta*, 755:1–16, 2012.

[14] A Manceau, KL Nagy, MA Marcus, M Lanson, N Geoffroy, T Jacquet, and T Kirpichtchikova. Formation of metallic copper nanoparticles at the soil- root interface. *Environmental Science and Technology*, 42(5):1766–1772, 2008.

[15] M Oakes, RJ Weber, B Lai, A Russell, and ED Ingall. Characterization of iron speciation in urban and rural single particles using xanes spectroscopy and micro x-ray fluorescence measurements: investigating the relationship between speciation and fractional iron solubility. *Atmospheric Chemistry and Physics*, 12(2):745–756, 2012.

[16] SR Walker, HE Jamieson, and PE Rasmussen. Application of synchrotron microprobe methods to solid-phase speciation of metals and metalloids in house dust. *Environmental Science and Technology*, 45(19):8233–8240, 2011.

[17] F Bardelli, G Barone, V Crupi, F Longo, D Majolino, P Mazzoleni, and V Venuti. Combined non-destructive xrf and sr-xas study of archaeological artefacts. *Analytical and Bioanalytical Chemistry*, 399(9):3147–3153, 2011.

[18] M West, AT Ellis, PJ Potts, C Streli, C Vanhoof, D Wegrzynek, and P Wobrauschek. Atomic spectrometry update: X-ray fluorescence spectrometry. *Journal of Analytical Atomic Spectrometry*, 25(10):1503–1545, 2010.

[19] Mt West, AT Ellis, PJ Potts, C Streli, C Vanhoof, D Wegrzynek, and P Wobrauschek. Atomic spectrometry update: X-ray fluorescence spectrometry. *Journal of Analytical Atomic Spectrometry*, 26(10):1919–1963, 2011.

[20] M West, AT Ellis, PJ Potts, C Streli, C Vanhoof, D Wegrzynek, and P Wobrauschek. Atomic spectrometry update: X-ray fluorescence spectrometry. *Journal of Analytical Atomic Spectrometry*, 27(10):1603–1644, 2012.

[21] M West, AT Ellis, PJ Potts, C Streli, C Vanhoof, D Wegrzynek, and P Wobrauschek. 2013 atomic spectrometry update: A review of advances in x-ray fluorescence spectrometry. *Journal of Analytical Atomic Spectrometry*, 28(10):1544–1590, 2013.

[22] A Iida. Synchrotron radiation x-ray fluorescence spectrometry. *Encyclopedia of Analytical Chemistry*.

[23] KE Limburg, R Huang, and DH Bilderback. Fish otolith trace element maps: new approaches with synchrotron microbeam x-ray fluorescence. *X-Ray Spectrometry*, 36(5):336–342, 2007.

[24] KD Perry, SS Cliff, and MP Jimenez-Cruz. Evidence for hygroscopic mineral dust particles from the intercontinental transport and chemical transformation experiment. *Journal of Geophysical Research: Atmospheres*, 109(D23), 2004.

[25] RA VanCuren, T Cahill, J Burkhart, D Barnes, Y Zhao, K Perry, S Cliff, and J McConnell. Aerosols and their sources at summit greenland–first results of continuous size-and time-resolved sampling. *Atmospheric Environment*, 52:82–97, 2012.

[26] TA Cahill, SS Cliff, KD Perry, M Jimenez-Cruz, G Bench, P Grant, D Ueda, JF Shackelford, M Dunlap, and M Meier. Analysis of aerosols from the world trade center collapse site, new york, october 2 to october 30, 2001. *Aerosol Science and Technology*, 38(2):165–183, 2004.

[27] G Bench, PG Grant, D Ueda, SS Cliff, KD Perry, and TA Cahill. The use of stim and pesa to measure profiles of aerosol mass and hydrogen content, respectively, across mylar rotating drums impactor samples. *Aerosol Science and Technology*, 36(5):642–651, 2002.

[28] N Bukowiecki, P Lienemann, CN Zwicky, M Furger, A Richard, G Falkenberg, K Rickers, D Grolimund, C Borca, and M Hill. X-ray fluorescence spectrometry for high throughput analysis of atmospheric aerosol samples: The benefits of synchrotron x-rays. *Spectrochimica Acta Part B: Atomic Spectroscopy*, 63(9):929–938, 2008.

[29] N Bukowiecki, P Lienemann, M Hill, M Furger, A Richard, F Amato, ASH Prévôt, U Baltensperger, B Buchmann, and R Gehrig. Pm10 emission factors for non-exhaust particles generated by road traffic in an urban street canyon and along a freeway in switzerland. *Atmospheric Environment*, 44(19):2330–2340, 2010.

[30] N Bukowiecki, P Lienemann, M Hill, R Figi, A Richard, M Furger, K Rickers, G Falkenberg, Y Zhao, and SS Cliff. Real-world emission factors for antimony and

other brake wear related trace elements: size-segregated values for light and heavy duty vehicles. *Environmental Science and Technology*, 43(21):8072–8078, 2009.

[31] A Richard, N Bukowiecki, P Lienemann, M Furger, M Fierz, MC Minguillón, B Weideli, R Figi, U Flechsig, and K Appel. Quantitative sampling and analysis of trace elements in atmospheric aerosols: impactor characterization and synchrotron-xrf mass calibration. *Atmospheric Measurement Techniques*, 3(5):1473–1485, 2010.

[32] A Richard, MFD Gianini, C Mohr, M Furger, N Bukowiecki, MC Minguillón, P Lienemann, U Flechsig, K Appel, and PF DeCarlo. Source apportionment of size and time resolved trace elements and organic aerosols from an urban courtyard site in switzerland. *Atmospheric Chemistry and Physics*, 11(17):8945–8963, 2011.

[33] R Ogawa, H Ochi, M Nishino, N Ichimaru, and R Yamato. Effect of primary filter using theoretical intensity of fluorescent x-rays and scattered x-rays. *X-Ray Spectrometry*, 39(6):399–406, 2010.

[34] R Cossio, G Vaggelli, and A Borghi. Improvements in trace element detection in energy dispersive spectrometry using an x-ray filter (feds) and applications to petrological problems. *Microchimica Acta*, 161(3-4):337–342, 2008.

[35] JT Gilmore. Use of a primary beam filter in x-ray fluorescence spectrometric determination of trace arsenic. *Analytical Chemistry*, 40(14):2230–2232, 1968.

[36] R Van Grieken and A Markowicz. *Handbook of X-ray Spectrometry*. CRC Press, 2001.

[37] TA Cahill. Proton microprobes and particle-induced x-ray analytical systems. *Annual Review of Nuclear and Particle Science*, 30(1):211–252, 1980.

[38] JS Iwanczyk, BE Patt, S Barkan, L Feng, and CR Tull. High throughput high resolution vortex detector for x-ray diffraction. *Nuclear Science, IEEE Transactions on*, 50(6):2470–2473, 2003.

[39] OG Raabe, DA Braaten, RL Axelbaum, SV Teague, and TA Cahill. Calibration studies of the drum impactor. *Journal of Aerosol Science*, 19(2):183–195, 1988.

[40] TA Cahill, TM Cahill, DE Barnes, NJ Spada, and R Miller. Inorganic and organic aerosols downwind of california's roseville railyard. *Aerosol Science and Technology*, 45(9):1049–1059, 2011.

Chapter 4
Conclusions

The analytical optimizations of the Synchrotron Radiation X-Ray Fluorescence (SR-XRF) technique at the Stanford Synchrotron Radiation Lightsource (SSRL) described in Chapters 2 and 3 of this thesis provide researchers with a method for non-destructively analyzing a wide variety of environmental samples with high elemental sensitivity and selectivity. Of the four methods (monochromatic beam, white beam, filtered white beam, and filtered white beam-filtered detector) tested during the experiments, the straight polychromatic white beam configuration resulted in the best sensitivity for elements across a large range of x-ray energies for small amounts of mass collected on thin film substrates. The simple addition of beam and detector filtering to the white beam configuration provided a method for selecting elements with more energetic x-rays. The result that the best sensitivity came from the white beam configuration was unexpected because the standard mode of operation for most SR-XRF analyses is a monochromatic beam, which gave the least sensitive analysis in the multi-substrate comparison detailed in this thesis.

The ability to modify the SR-XRF analysis technique to select for specific elements in samples containing small amounts of mass, such as aerosol samples collected on thin films, solves one of the technical challenges inherent in analyzing the temporal variability of environmental aerosol samples. The temporal variability of aerosol samples collected by aerosol impactors, such as the DRUM samplers described in chapter 2, is limited by the sensitivity of the analysis technique. Less sensitive techniques require a large sample spot, which was collected over a larger period of time, to be analyzed to get enough mass to detect the elements of interest. If the analysis technique is more sensitive, a smaller spot, corresponding to a shorter time step, can provide the elemental concentrations with the same certainty.

As described in Chapter 1, the spatial resolution of aerosol concentration samples collected along an unmanned aircraft system's (UAS's) flight path also is limited by the sensitivity of the analysis technique. In UAS operations, the length of the aerosol sample spot corresponds to a distance, so the SR-XRF optimizations described in this thesis that decrease the amount of sample mass required for detectable elemental concentrations allows the aerosol samples to be analyzed in smaller time steps. Smaller time steps result in a higher spatial resolution for the aerosol measurements. Additionally, if the aerosol contains a high-energy, x-ray emitting element of interest, such as a heavy metal in a plume

from an industrial source like a car shredder, the analysis can be optimized through the use of beam and detector filters to preferentially detect that element.

The optimizations of the SR-XRF technique described in this thesis allow for the higher temporal and spatial resolution of atmospheric aerosol concentrations. They also enhance the suite of non-destructive, element-specific analyses available for answering scientific questions about historical documents, meteorites, and other irreplaceable and valuable samples.

4.1 Future Work

The optimization of the analytical technique described in this thesis provides a foundation for diverse scientific studies and other follow-on work. However, before any long-term sample analysis program begins, the SSRL beamline 2-2 system for the white beam analyses of thin-film aerosol samples should be the focus of some engineering expertise. The analysis chamber, beam and detector filter holders, detector mount, stage locomotion drive, and sample holder need to be made sturdier and less able to be jostled out of alignment. This will improve the reproducibility of the sample analyses and the ease of adding and removing beam and detector filters. Additionally, the software that runs the stage locomotion driver should be improved and combined with the detector software so spectra can be viewed as the beam moves along the sample stage. A laser pointer for identifying the location of the beam spot on the sample would provide improved alignment of the system.

Running additional optimization scenarios would provide a table of optimization settings for each potential element. This will allow scientists interested in a specific element of interest to simply look up the beam and detector-filtering scenario that will provide them with the best sensitivity for their species of interest.

The SR-XRF technique's elemental sensitivity calculations should be applied to theoretical DRUM impactor sample resolutions to identify the smallest temporal step obtainable for select elements under different atmospheric aerosol loading conditions. The results of this analysis will allow the samplers to be optimized for the ambient aerosol conditions where they are deployed, leading to fewer incidences of over or under-loading the sample and degrading the information from the sampler.

The development of the Airborne DRUM Sampler (ADS) provides an opportunity to use the high sensitivity of the optimized SR-XRF to obtain highly spatially resolved aerosol

composition from a UAS. The sensitivity of the technique will decrease the amount of time, and associated distance travelled, needed to collect enough mass to analyze for elemental composition. If the UAS also contains an optical particle counter or some other real-time particulate matter concentration instrument, the data from that instrument could be used to change the collection time for the ADS on the fly. Changing the collection time of the sampler during a flight could guarantee high quality aerosol measurements along a flight path that includes both high and low aerosol concentrations, such as through a smoke plume and in the clean air on either side.

The aerosol samples collected during sampling flights and analyzed by the optimized SR-XRF technique will provide unique and important information on the three-dimensional aerosol environment and how it changes with time. This information is needed to validate satellite aerosol algorithms, initialize or confirm atmospheric dispersion models, quantify the impact of aerosols on the Earth's radiative balance, determine the causes and distribution of high concentrations of air pollution, track volcanic plumes, and assist in understanding and solving numerous other environmental questions. Although optimizing the SR-XRF technique at SSRL for aerosol samples may not seem as though it can have far-reaching impacts, it produces information of importance across the scientific community.